Aspects of Molecular Medicine 5 (2025) 100080

Contents lists available at ScienceDirect

Aspects of Molecular Medicine

journal homepage: www.journals.elsevier.com/aspects-of-molecular-medicine

Evaluation of inhibitory efficacy of plantaricin JK against NSP1 from SARS-CoV-2 by *in silico* methods

Manisha Mandal [a], Shyamapada Mandal [b,*]

[a] Department of Physiology, MGM Medical College, Kishanganj, Bihar, PIN-855107, India
[b] Department of Zoology, University of Gour Banga, West Bengal, Malda, PIN-732103, India

ARTICLE INFO

Handling Editor: Prof A Angelo Azzi

Keywords:
SARS-CoV-2
Non-structural protein-1
Plantaricin JK
Peptide 5
Molecular docking
Molecular dynamic simulation
MM-GB(PB)SA binding free energy

ABSTRACT

SARS-CoV-2 (severe acute respiratory syndrome coronavirus 2), the causative agent of the COVID-19 pandemic, is still a cause of global concern, and therefore, safe and effective treatment is desperately needed. Bacteriocins produced by probiotic microorganisms displayed therapeutic potentiality against infectious diseases, including COVID-19. NSP1 (non-structural protein-1) of SARS-CoV-2 acts as a host translation inhibitor and reduces host immune function, thereby increasing viral pathogenicity and virulence. This information encouraged us to evaluate the inhibitory role of plantaricin JK (Pln-JK) against SARS-CoV-2 NSP1 using *in silico* methods. Herein, we used PatchMAN and CABS-dock webtools to perform molecular docking between SARS-CoV-2 NSP1 and Pln-JK, which generated NSP1-Pln-JK models. We used a peptide antiviral, peptide 5 (PEP5) as a reference. The top models (based on the lowest binding score and cluster density) of both systems were subjected to predict the binding affinity (ΔG, kcal/mol) and dissociation constant (K_D, M) using PRODIGY. Pln-JK had excellent interaction with NSP1 displaying binding affinity of 9.1 kcal/mol and K_D value of 2.1×10^{-7}. The binding affinity and K_D values for NSP1-PEP5 were −7.2 kcal/mol and 4.8×10^{-6} M (for PatchMan complex) and −5.9 kcal/mol and 4.8×10^{-5} M (for CABS-dock complex), respectively. HawkDock-based MM-GBSA binding free energies of CABS-dock and PatchMAN-generated complexes were −59.74 and −77.49 kcal/mol (for NSP1-Pln-JK) and −37.83 and −44.25 kcal/mol (for NSP1-PEP5), respectively. Further, molecular dynamic simulations-based MM-PBSA binding free energy confirmed NSP1-Pln-JK complex (−31.89 ± 0.91 kcal/mol) to be thermodynamically more stable than NSP1-PEP5 complex (−24.94 ± 0.6 kcal/mol). Pln-JK was predicted as non-allergic and non-toxic and thus emerged as a safe and effective molecule to combat SARS-CoV-2 infection. However, preclinical and clinical studies are needed before it can be considered as a prescription drug for the treatment of COVID-19.

1. Introduction

The COVID-19 pandemic was caused by the infection with a member of the genus *Betacoronavirus* (family: Coronaviridae) called SARS-CoV-2 (Severe Acute Respiratory Syndrome Coronavirus 2)— a positive-sense single-stranded RNA virus. The COVID-19 pandemic, which originated in China, is one of the world's 21st-century challenges. As of November 24, 2024, a total of 776,947,553 cases and 7,076,993 deaths of COVID-19 have been reported to WHO (https://data.who.int/dashboards/covid19/data), and the disease is still a cause of global concern. This is due to the lack of specific anti-SARS-CoV-2 treatment. These data emphasize the need to develop safe and effective drugs for COVID-19 treatment.

The SARS-CoV-2 genome of ~30 kb contains 14 open reading frames (ORFs) grouped into ORF1a and ORF1ab, which are translated into two polyproteins: pp1a and pp1ab (Arya et al., 2021). These polyproteins are cleaved, by two viral proteases: papain-like protease (PLpro) and main-protease (Mpro), into 16 non-structural proteins (NSPs), NSP1 to NSP16 (Chen et al., 2020). The NSP1, among 16 NSPs, inhibits the host cell protein synthesis by binding to the host 40S ribosomes, induces endonucleolytic cleavage of host mRNA, and evades the innate immune defense of the host (Chen et al., 2020; Kamitani et al., 2009). NSP1 is crucial to play a role in the process of SARS-CoV-2 replication inside the human host and has been an essential virulence factor (Yan et al., 2022), which increases pathogenicity (KC, 2024). The vital role of the NSP1 protein in the SARS-COV-2 life cycle has made it an important target for the development of antiviral therapy (Min et al., 2020; Ma et al., 2022; Thoms et al., 2020).

* Corresponding author.
E-mail addresses: debmanisha@rediffmail.com (M. Mandal), samtropmed@gmail.com, sam.micro11@ugb.ac.in (S. Mandal).

https://doi.org/10.1016/j.amolm.2025.100080
Received 19 December 2024; Received in revised form 27 March 2025; Accepted 27 March 2025
Available online 28 March 2025

Previous authors explained small-molecule-based drug development for the treatment of COVID-19 caused by the infection of SARS-CoV-2 by *in silico* approaches (Bhardwaj et al., 2021). The researchers have demonstrated how molecular docking is crucial to predict the binding affinity of phytochemical ligands to different target proteins from SARS-CoV-2, and how proteins interact with ligands involving different amino acid residues to form stable protein-ligand complexes defining the most active inhibitors for a particular protein (Singh and Purohit, 2024; Bhardwaj et al., 2021). It has been explained previously how molecular dynamics simulation (MDS) helps confirm the conformational stability of docked complex, and MM-PB(GB)SA binding free energies are crucial to justify the thermodynamic stability of the complex (Singh et al., 2021b; Bhardwaj et al., 2021; Mandal and Mandal, 2024a). Furthermore, the importance of applying of computational biology tools that help predict the drug-like properties, bioavailability, pharmacokinetics and toxicity of ligands (bioactive compounds) to identify the safe drug candidates has been explained. Sing et al. (2022) reported the anti-SARS-CoV-2 efficacy of curcuminoid-based small-molecules using *in silico* methods by targeting NSP15. For this purpose, the authors performed molecular docking, MDS, MM-PBSA binding free energy calculations, and pharmacokinetics property analysis. The SARS-CoV-2 RdRp-RNA was targeted for anti-COVID-19 drug development by *in silico* molecular docking, MDS and computation of binding free energies by using the same set of phytochemicals, curcuminoids (Singh et al., 2021a). Sharma et al. (2021b) reported NSP15-targeted anti--SARS-CoV-2 activities of bioactive phytochemicals (kaempferol, barrigenol and myricetin) using molecular docking, MDS and binding free energy calculations by MM-PBSA analysis.

In modern drug discovery platforms, molecular docking is performed computationally to predict the binding affinity between target protein and ligands (small molecules or peptides) and to confirm the energetic stability of the protein-ligand docked complexes by MM-GBSA binding free energy calculations (Mandal and Mandal, 2024a, 2024b). Targeting the NSP1virulence factor of SARS-CoV-2, ligands bearing the ChEMBL identifiers, CHEMBL1096281, CHEMBL2022920, CHEMBL175656, had the best binding affinity values with NSP1 (Chowdhury and Bagchi, 2022). Small-molecule ligands (N-feruloyltyramine, beta-Sitosterol, 13-(1,3-benzodioxol-5-yl)-N-(2methylpropyl) trideca-2,4,12-trienamide, and N-(2-methylpropyl) octadeca-2-4dienamide from *Piper sarmentosum* have been reported to exhibit inhibitory activity against SARS-CoV-2 NSP1 (KC et al., 2024). Several other authors demonstrated anti-SARS-CoV-2 drug discovery (small-molecular weight compounds) by targeting NSP1 (Gi Byun et al., 2024; Sundar et al., 2021; De Lima Menezes and Da Silva, 2021). Similar to the small molecular-weight ligands mentioned above, antimicrobial peptides (AMPs) including bacteriocins have also been investigated for COVID-19 drug discovery (Dey et al., 2021), targeting different proteins from SARS-CoV-2, such as protease (Razali et al., 2021; Erol et al., 2023) and S protein receptor binding domain (Teiar et al., 2024). Two bacteriocins, glycocin F (from *Lactococcus lactis*) and lactococcine G (from *Lactobacillus plantarum*) showed high efficacy against RdRp, 3CL, S, and N proteins of SARS-CoV-2 (Balmeh et al., 2021).

The plantaricin bacteriocins are safe AMPs produced by probiotic lactobacilli, *Lactobacillus plantarum* stains (Abdulhussain and Razavi, 2020). The antiviral, including anti-SARS-CoV-2, activities of different plantaricins have been reported earlier (Omer et al., 2022; Dassanayake et al., 2022; Kim et al., 2020). A class IIb bacteriocin, plantaricin JK (Pln-JK) derived from *Lactobacillus plantarum* C11 (Rogne et al., 2009), exhibited inhibitory activity against bacterial pathogens as reported earlier (Xu et al., 2019; Chaalel et al., 2015). One of the most important properties of Pln-JK is that this is a two-peptide bacteriocin produced by *Lactobacillus plantarum* (Anderssen et al., 1998), which is an excellent probiotic suitable for human consumption (Echegaray et al., 2023; Aljohani et al., 2024). Moreover, it is amphipathic with net positive charge, and exhibits strong attraction to the negatively charged membrane structures of pathogens, causing disruption of membrane integrity by pore formation leading to cell death (Moll et al., 1999). This phenomenon has been applicable for the two peptide bacteriocin, as reported earlier in Pln-NC8 αβ (Omer et al., 2022). Further, Pln-JK has been reported as 10^3 times more active at nanomolar concentrations than the individual activities of Pln-J and Pln-K (Anderssen et al., 1998). Another two-peptide class IIb bacteriocin derived from *L. plantarum* named Pln-NC8 αβ exhibits very strong activities at nanomolar (nM) to micromolar (μM) concentrations against influenza A virus as well as coronavirus SARS-CoV-2 (Omer et al., 2022). Being a two-peptide class IIb bacteriocin Pln-JK may therefore possess antiviral efficacy with similar potential against SARS-CoV-2. Besides, Pln-JK has demonstrated antiviral activity against Flavivirus, KUNV (Kunjin virus), and when combined with another two-peptide bacteriocin, Pln-EF had synergistic action at 10 μM, resulting in >99.9 % reduction in viral load (Omer et al., 2025).

However, the AMPs including Pln-JK bacteriocin have not been studied against NSP1 of SARS-CoV-2. Therefore, the current study aims to determine the anti-SARS-CoV-2 activity of Pln-JK for structure-based drug development targeting NSP1 using computational biology tools. Herein, we performed molecular dockings to predict the binding affinity of Pln-JK against SARS-CoV-2 NSP1. This study also predicted the energetically stable NSP1-Pln-JK complex formation by binding free energy calculations using MM-GBSA and MM-PBSA approaches. Finally, we have done safety profiling of Pln-JK bacteriocin by *in silico* physicochemical property analysis, and allergenicity and toxicity testing.

2. Materials and methods

2.1. Target protein and peptide inhibitor

The SARS-CoV-2 non-structural protein-1 (NSP1), also known as host translation inhibitor, was selected as a druggable target for the current study. From RCSB PDB (protein data bank), the X-ray diffraction structure of NSP1 (resolution: 1.18 Å) PDB file (PDB ID: 8AZ8; Version 1.0: 2022-11-23) was retrieved (https://www.rcsb.org/structure/8AZ8) (Ma et al., 2022).

The bacteriocin called Plantaricin JK (Pln-JK) composed of 25 amino acid residues (sequence: GAWKNFWSSLRKGFYDGEAGRAIRR) was selected as a peptide ligand. The information on Pln-JK was obtained from YADAMP (Yet Another Database of Antimicrobial Peptides) (http://yadamp.unisa.it/default.aspx), an antimicrobial peptide database (Piotto et al., 2012), with detailed information for **2525** manually annotated peptide sequences (As of January 9, 2024).

We have utilized a reference antiviral peptide, peptide 5 (PEP5) composed of 15 amino acid residues (sequence: IYALLENAEDYNLVN), obtained from DRAVP (data repository of antiviral peptides and proteins) (http://dravp.cpu-bioinfor.org/). PEP5 is a synthetic construct that inhibit the SARS-CoV-2 entry in host cell by antagonizing the ACE-2 (angiotensin-converting enzyme-2) interaction with RBD (receptor binding domain) of SARS-CoV-2 spike protein (Sadremomtaz et al., 2022).

The NSP1protein model structure was validated by overall quality factor estimation using ERRAT2 program, and the Ramachandran plot analysis using PROCHECK, both accessible from the webserver, SAVES v6.0 (https://saves.mbi.ucla.edu/). Further, we operated the ProSA webserver (https://prosa.services.came.sbg.ac.at/prosa.php) to predict the Z score of NSP1.

2.2. Protein-peptide docking

The bacteriocin Pln-JK was docked to SARS-CoV-2 NSP1 protein by using PatchMAN (Patch-Motif AligNments) webserver (https://furmanlab.cs.huji.ac.il/patchman/), which provides a novel approach for high-resolution global protein-peptide docking (Leffler et al., 2017). To run the systems the receptor protein PDB file and peptide ligand (bacteriocin) sequence was used as the inputs. The initial structures were processed to refine using the Rosetta FlexPepDock refinement

protocol, and the top-scoring model was selected for further predictions. We have also performed a second docking, and for this purpose CABS-dock (http://biocomp.chem.uw.edu.pl/CABSdock/) web server (Blaszczyk et al., 2019), which provides a tool for flexible docking of peptides to proteins, was used. The CABS-dock docking, using the input files (protein receptor structure (.PDB) and peptide (Pln-JK) sequence of 4–30 residues), search for the binding site favouring the full flexibility of the peptide and small fluctuations of the receptor backbone. By clustering and scoring, this system generates 10 top-scored low-energy models, and we have selected one displaying the lowest average RMSD value with the highest cluster density, for further analysis. Subsequently, for comparison of the anti-SARS-CoV-2 efficacy we carried out docking between SARS-CoV-2 NSP1 protein and PEP5 reference antiviral using both the PatchMAN and CABS-dock webtools, as explained for Pln-JK.

Furthermore, we performed another global docking using the ClusPro server (https://cluspro.org) to verify the results obtained from PatchMAN and CABS-dock dockings in terms of binding energy of the NSP1-Pln-JK and NSP1-PEP5 complexes (generated from PatchMAN and CABS-dock docking). The ClusPro docking provides models defined by centres displaying various clusters of different members with low-energy docked structures (Kozakov et al., 2017). We used GPU server option and other default parameters to accomplish the ClusPro docking.

2.3. Binding affinity and K_D prediction

The top-ranked protein-peptide (NSP1-Pln-JK) docked complexes were retrieved from both the systems: PatchMAN docking and CABS-dock docking, as explained above, for the prediction of binding affinity (ΔG, kcal/mol) and dissociation constant (K_D, M) between SARS-COV-2 NSP1 and bacteriocin Pln-JK. For the job accomplishment, we utilized the PRODIGY (Protein Binding Energy Prediction) (https://wenmr.science.uu.nl/prodigy/) webserver, as reported previously (Mandal and Mandal, 2024a). The PRODIGY server highly effective predictive model based on intermolecular contacts and properties resulting from non-interface surfaces. To compare the Pln-JK effectiveness against SARS-COV-2 NSP1, binding affinity and K_D values were predicted also for NSP1-PEP5 top-ranked complexes from PatchMAN docking as well as CABS-dock docking by using PRODIGY as explained above.

2.4. Intermolecular (protein-peptide) interaction

The top-ranked NSP1-Pln-JK complex (.pdb), both from CABS-dock docking and from PatchMAN docking, was subjected to intermolecular interaction analysis. After the PRODIGY analysis NSP1-Pln-JK complexes were viewed in PyMol version 2.5.4 (https://pymol.org/2/) and analysed using PyMol ICs-based representation (Mandal and Mandal, 2024a). For 2-D intermolecular interactions analysis of NSP1-Pln-JK complexes was accomplished by using the DIMPLOT of Ligplot + v.2.2.7 (https://www.ebi.ac.uk/thornton-srv/software/LigPlus/) tool (Laskowski and Swindells, 2011). The PDBsum generate (http://www.ebi.ac.uk/thornton-srv/databases/pdbsum/Generate.html) webtool was used for the structural validation of the complexes, and for mapping the interacting residues at the protein-peptide interfaces (Laskowski et al., 2018). Further, we used the BIOVIA Discovery Studio v21.1.0.20298 (https://www.3ds.com/products-services/biovia/products/molecular-modeling-simulation/biovia-discovery-studio/visualization/), to analyse the intermolecular interactions of PatchMan-generated NSP1-Pln-JK and NSP1-PEP5 complexes for the elucidation of protein-peptide interaction map.

2.5. MM-GBSA binding free energy estimation

The top-ranked NSP1-Pln-JK docked complexes retrieved from PatchMAN docking as well as CABS-dock docking systems were subjected to free binding energy computation by MM-GBSA (Molecular Mechanics with Generalized Born and Surface Area) approach to compare the energetic stability of the complexes formed between Pln-JK and NSP1 in two different docking systems. We have selected model 1 from both the systems (PatchMAN docking as well as CABS-dock docking), and were uploaded to the HawkDock webserver (http://cadd.zju.edu.cn/hawkdock/), which estimates global (total) binding free energies ($\Delta G_{bind\ (MM\text{-}GBSA)}$) and decomforse the free energy contributions to the binding free energy of a protein-protein complex in per-residue basis (Mandal and Mandal, 2024a). As described above for NSP1-Pln-JK complexes, the HawkDock-based MM-GBSA binding free energy calculations were done also for top-ranked NSP1-PEP5 complexes, generated both from PatchMAN docking and CABS-dock docking, for comparison. Thereafter, the NSP1-Pln-JK and NSP1-PEP5 complexes exhibiting lowest MM-GBSA binding free energy were subjected to further analysis for MDS and MM-PBSA binding free energy calculations.

2.6. Molecular dynamics simulation and MM-PBSA binding free energy calculations

NSP1-Pln-JK and NSP1-PEP5 complexes obtained from PatchMAN docking had lower MM-GBSA binding free energy than the NSP1-Pln-JK and NSP1-PEP5 complexes generated from CABS-dock docking, and therefore the PatchMAN-derived complexes were selected for MDS and MM-PBSA binding free energy calculations. The MDS was carried out using GROMACS (version 2022.3) software (https://www.gromacs.org), as detailed earlier (Mandal and Mandal, 2024b). After completing MDS for 10 ns, the trajectories were analysed to measure various metrices: root mean square deviation (RMSD), root mean square fluctuation (RMSF), solvent-accessible surface area (SASA) and radius of gyration (Rg) for both the complexes, NSP1-Pln-JK and NSP1-PEP5, in order to confirm the conformational stability of the complexes. Additionally, we analysed the free energy of solvation for the MDS trajectories.

Further, the PatchMAN-derived NSP1-Pln-JK and NSP1-PEP5 complex trajectories were analysed for the calculation of MM-PBSA (Molecular mechanics-Poisson-Boltzmann surface area) binding free energy to confirm which one of the complexes was energetically more stable. The gmx_MMPBSA v1.6.0 tool (https://valdes-tresanco-ms.github.io/gmx_MMPBSA/v1.6.0/) (Valdés-Tresanco et al., 2021), as provided with MMPBSA.py v.16.0 program found in the AmberTools22 package (https://ambermd.org/) (Miller et al., 2012), was used to accomplish the process. We have explained the system details earlier (Mandal and Mandal, 2024b).

2.7. Peptide safety and toxicity profiling

The bacteriocin Pln-JK and reference antiviral PEP5 were subjected to physicochemical property analysis using PepCalc webserver (https://pepcalc.com/) (Lear and Cobb, 2016), which estimates molecular weight, iso-electric point, net charge, extinction coefficient and solubility of peptide molecules. To predict the oral bioavailability of Pln-JK and PEP5, a publicly accessible webtool, ADMETboost, available at: https://ai-druglab.smu.edu/admet, was used, while the peptide stability prediction tool, available at: https://peptidestability.crg.eu/, was used to predict the physical stability of Pln-JK and PEP5. The peptide stability prediction tool is trained with a machine-learning model to provide knowledge about the physical stability of the peptide, an important feature to justify the therapeutic quality of peptide drugs before experimental validation. This tool requires an amino acid sequence as input to accomplish the prediction.

For allergenicity testing of the bacteriocin and the reference antiviral peptide (PEP5), we have utilized AlgPred 2.0 (https://webs.iiitd.edu.in/raghava/algpred2/) predicting allergenic proteins by different techniques, such as prediction of allergen (machine learning approach by Random Forest), mapping of IgE epitopes, mapping of motifs, and

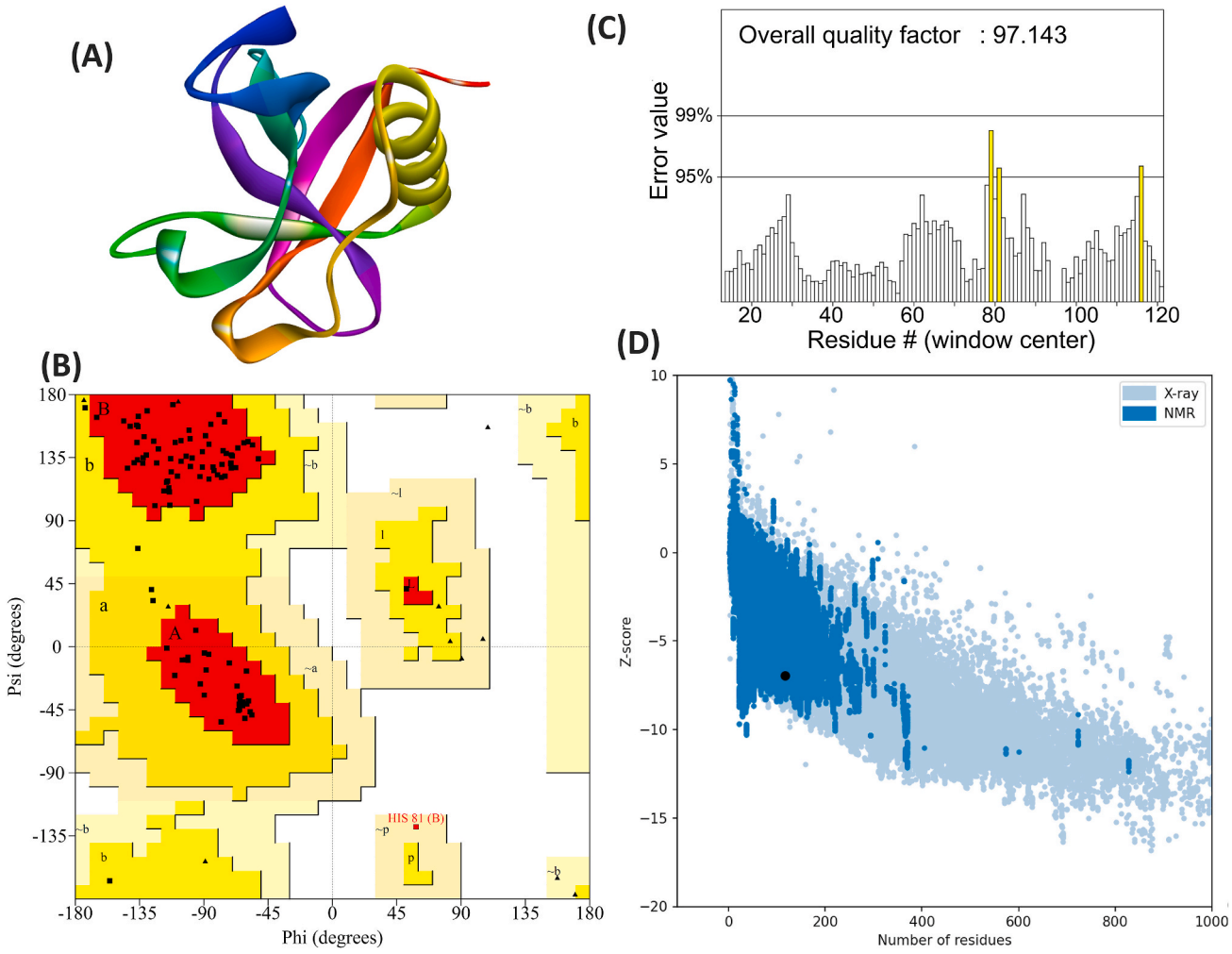

Fig. 1. The SARS-CoV-2 (severe acute respiratory syndrome coronavirus 2) NSP1 (non-structural protein-1) target protein and structural validation of the model. (A) 3-D structure (B) Ramachandran plot of NSP1 with 93.9 % residues in the most favoured region (C) ERRAT2-generated overall quality factor of the model (D) Z-score plot for the model protein.

searching similarity by BLAST (Sharma et al., 201a). For toxicity prediction of Pln-JK and PEP5, CSM-Toxin (https://biosig.lab.uq.edu.au/csm_toxin) (Morozov et al., 2023) and ToxinPred (http://crdd.osdd.net/raghava/toxinpred/) (Gupta et al., 2013) webservers were utilized.

3. Results and discussion

In order to predict accurately the binding capacity of Pln-JK to NSP1 we accomplished protein-peptide docking using two systems: PatchMan (Khramushin et al., 2022) and CABS-dock (Kurcinski et al., 2015), both of which perform global docking that provides full flexibility of the receptor protein (herein NSP1 from SARS-CoV-2) and peptide (herein Pln-JK from *Lactobacillus plantarum* C11), and generate models of large conformations by cluster-based scoring. Therefore, these two methods complement each other to validate the results. Docking between NSP1 and the reference antiviral peptide, PEP5, was also performed following PatchMan and CABS-dock for comparison. Additionally, we performed another global docking using the ClusPro server (https://cluspro.org) (Kozakov et al., 2017), to verify the results obtained from PatchMAN and CABS-dock dockings in terms of binding energy of the NSP1-Pln-JK and NSP1-PEP5 complexes (generated from PatchMAN and CABS-dock docking). In this connection, the top-ranked docked complexes were subjected to PRODIGY (Xue et al., 2016) for binding affinity and dissociation constant calculations, and then MM-GBSA binding free energy estimation was done. Finally, we accomplished molecular dynamics simulations, and thereafter the MM-PBSA-based binding free energy calculations were done to check the conformational as well as the energetic stability of the docked complexes. This is as explained below.

3.1. Protein model quality and structural authenticity

The PROCHECK and ProSA webtools provide an excellent platform for the analysis of protein model quality in computational drug development (Morris et al., 1992; Mercado-Camargo et al., 2020; Mandal and Mandal, 2024c). Herein, we have targeted the SARS-CoV-2 NSP1 protein, which was subjected to Ramachandran plot analysis and Z-score prediction for 3-D structure authentication of the protein. The Ramachandran plot, for NSP1 from SARS-CoV-2 (Fig. 1A), as analysed through PROCHECK revealed the presence of 93.9 % amino acids within the most favoured regions (Fig. 1B), which had an overall quality factor of 97.14, as analysed using ERRAT2 programme (Fig. 1C). The remaining 5.1 % and 1 % amino acids of NSP1 were found in the allowed and generously allowed regions (Fig. 1B), respectively. The ProSA-generated Z-score of the target protein was computed as −6.95 (Fig. 1D). In the current study, the NSP1 model did not exhibit any residues in the disallowed region of the Ramachandran plot, wherein Zero outliers best predict a high-quality protein model (Sobolev et al., 2020), and this feature has suitably clarified the selection of a target protein 3-D structure of good quality to perform computational drug development studies to perform efficient docking for obtaining precise

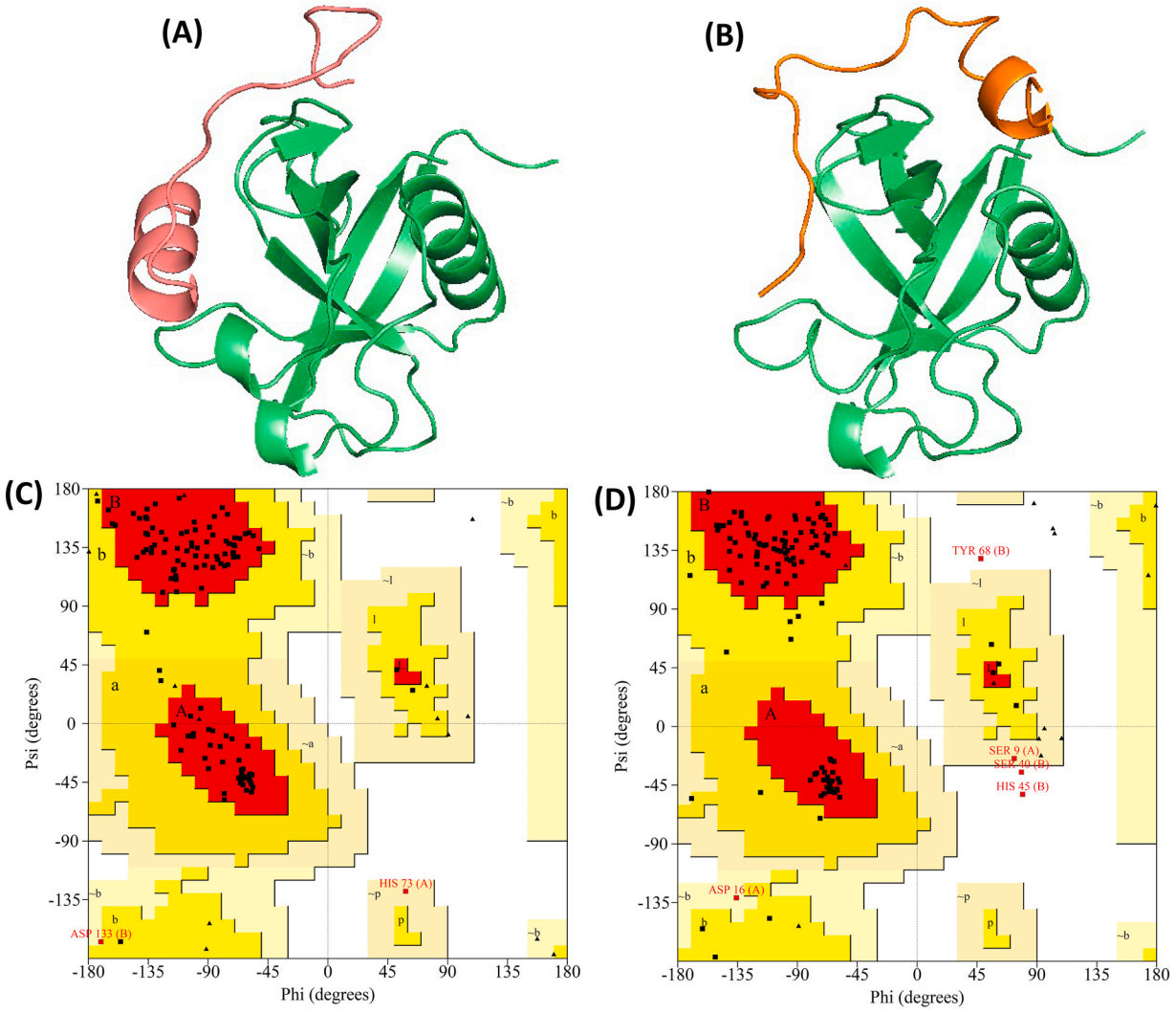

Fig. 2. The NSP1-Pln-JK docked complexes (A) PatchMan-generated complex between NSP1 (lime green) and Pln-JK (raspberry colour) (B) CABS-Dock-generated complex between NSP1 (lime green) and Pln-JK (orange colour) (C) Ramachandran plot of PatchMan-generated NSP1-Pln-JK complex with 93.2 %% residues in the most favoured region (D) Ramachandran plot of CABS-Dock-generated NSP1-Pln-JK complex with 83.1 % residues in the most favoured region. (For interpretation of the references to colour in this figure legend, the reader is referred to the Web version of this article.)

results. As previously explained, the acceptable Z-score generated using ProSA is < 0.5 (Mercado-Camargo et al., 2020), and in the instant study we predicted a score of −6.95 for SARS-CoV-2 NSP1, which falls within the array of model values obtained through experiments (X-ray/NMR) that further validate the structural quality of the target protein (Majumdar and Mandal, 2024). Thus, the model quality of the protein we used was favourable for molecular docking studies (Agnihotry et al., 2022; Mandal and Mandal, 2024c).

3.2. Molecular docking analysis

Previous authors targeted various proteins from SARS-CoV-2 for the development of peptide-based anti-COVID-19 therapy (Ramirez-Acosta et al., 2022; Jin et al., 2024; Lee et al., 2024). In the current study, among top 10 docked complexes, model 1 of the NSP1-Pln-JK complex with the lowest reweighted score of −340.887 and interface score of −36.709) was retrieved from PatchMAN docking. On the other hand, model 1 of NSP1-Pln-JK complexes generated from CABS-dock with the lowest average of RMSD 4.46 Å (cluster density: 26.41; number of elements: 118) was retrieved. The NSP1-Pln-JK complexes (model 1 from both the systems), and their Ramachandran plots are shown in Fig. 2. Fig. 3 shows the NSP1-PEP5 complex, as generated from PatchMAN docking and CABS-dock docking (model 1 from the both), along with their Ramachandran plots. PatchMAN-generated NSP1-PEP5 complex had a reweighted score of −337.247 and interface score of −36.208, while the NSP1-PEP5 complex (model 1: lowest average of RMSD 5.54 Å) selected from CABS-dock belonged to the cluster 1 having a cluster density of 31.97 and 177 members. To confirm the binding capacity, against the NSP1 protein, of both Pln-JK and PEP5, we conducted ClusPro docking (Fig. S1 and Fig. S2), the energy values of which are shown in Table 1. In case of PatchMan-generated docked complexes, NSP1-Pln-JK displayed binding energy of −906.2 kcal/mol, while the value was −555.6 kcal/mol for NSP1-PEP5, and in case of CABS-dock-generated complexes, the binding energies were −917.5 and −833.5 kcal/mol for NSP1-Pln-JK and NSP1-PEP5, respectively. Hence, ClusPro-generated energy values provide strong evidence for the efficacy of both Pln-JK and PEP5 against NSP1, although distinctions are seen between the energy values of the NSP1-Pln-JK complexes and the NSP1-PEP5 complexes. Therefore, the Pln-JK was more active to inhibit NSP1 protein than PEP5, as validated with CLusPro docking. Three peptides, such as P7 (RAWTFLDKFNHEAEDLRYQSSLASWN), P13 (RASTFLDKFNHEAEDLRYQSSLASWN) and P19 (RADTFLDKFNHEAEDLRYQSSLASWN) had been demonstrated to inhibit the RBD (receptor-binding domain) of SARS-CoV-2 spike protein (Pourmand

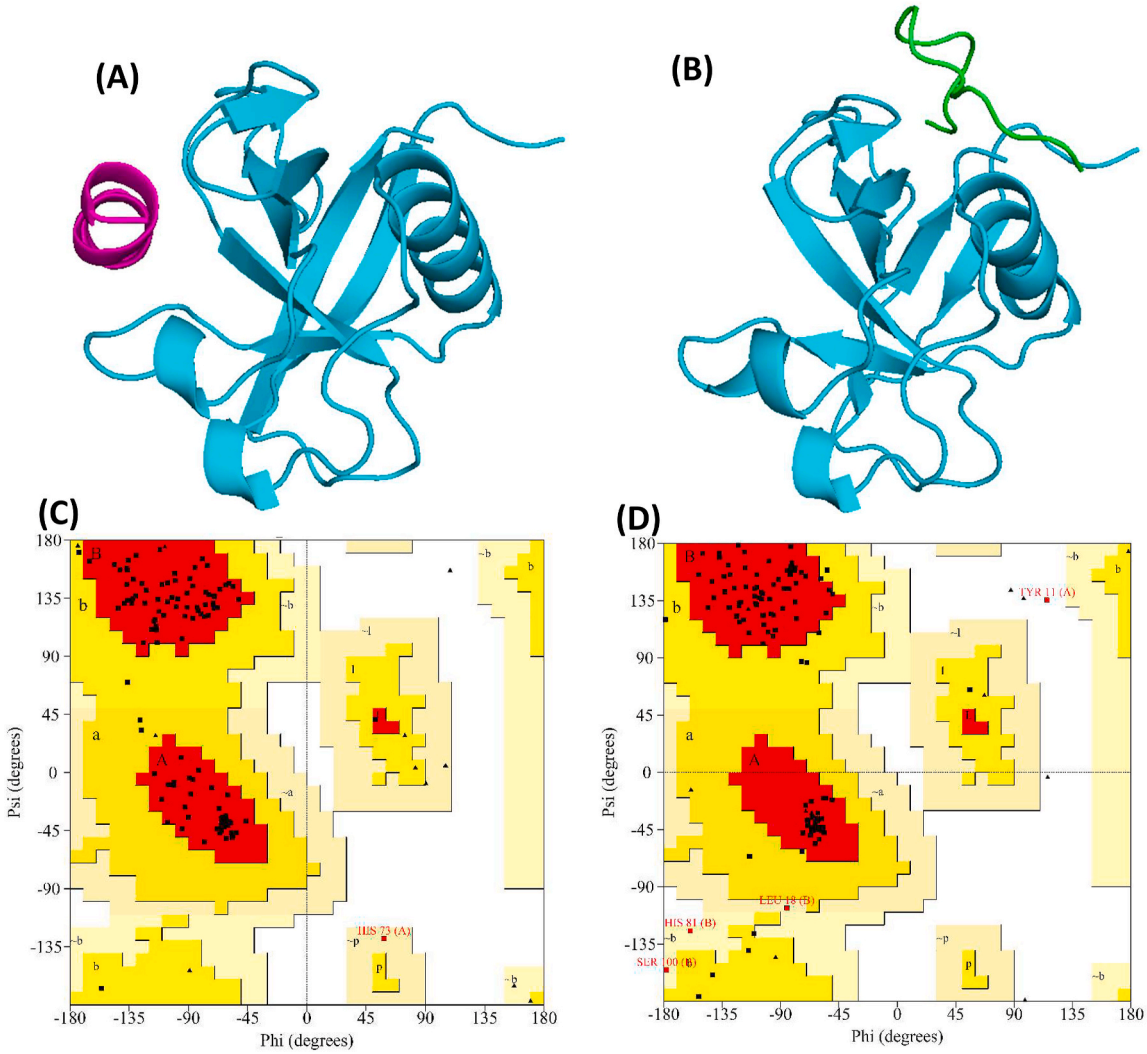

Fig. 3. The NSP1-PEP5 docked complexes (A) PatchMan-generated complex between NSP1 (blue) and PEP5 (magenta colour) (B) CABS-Dock-generated complex between NSP1 (blue) and PEP5 (green) (C) Ramachandran plot of PatchMan-generated NSP1-PEP5 complex with 94.6 %% residues in the most favoured region (D) Ramachandran plot of CABS-Dock-generated NSP1-PEP5 complex with 84.5 % residues in the most favoured region. (For interpretation of the references to colour in this figure legend, the reader is referred to the Web version of this article.)

Table 1
The ClusPro-derived docked complexes between NSP1 and Pln-JK/PEP5 retrieved from best clusters of highest members with centres and lowest docking scores (kcal/mol).

Protein-Peptide complex[a]	Cluster	Members	Representative	Weighted score
NSP1-Pln-JK (CABS-dock generated)	0	148	Centre	−837.2
			Lowest Energy	−917.5
NSP1-Pln-JK (PatchMan generated)	1	77	Centre	−906.2
			Lowest Energy	−906.2
NSP1-PEP5 (CABS-dock generated)	1	157	Centre	−833.5
			Lowest Energy	−867.4
NSP1-PEP5 (PatchMan generated)	3	106	Centre	−454.1
			Lowest Energy	−555.6

[a] The CABS-dock and PatchMan-generated models (protein and peptides) were used as inputs to accomplish ClusPro docking. PEP5: peptide 5; Pln-JK: plantaricin JK; NSP1: non-structural protein-1 of SARS-CoV-2.

et al., 2022). Peptide inhibitors (VPHW and DENPRHF) from hazelnut against SARS-CoV-2 proteases have been developed using CABS-dock (Güneş et al., 2024). The CLusPro docking was used to demonstrate the anti-SARS-CoV-2 activity of a fruit-derived peptide, bromelain, by targeting RBD proteins (Tallei et al., 2021). Different bacteriocins, such as glycocin F (−155.3 kcal/mol), tyrocidine A (−13.1 kcal/mol), gramicidin S (−11.4 kcal/mol) showed inhibitory properties against SARS-CoV-2 proteases by molecular docking (Razali et al., 2021).

As explained above, to confirm the binding efficiency of Pln-JK compared to PEP5, we performed dockings using different systems, such as PatchMAN, CABS-dock and ClusPro. All three of these perform global docking, and provide clusters by generating models (protein-peptide complexes) with different conformations of a ligand, wherein the ClusPro provides low energy information of docked structures (Kozakov et al., 2017), PatchMAN gives reweighted scores and ranks the models accordingly (Khramushin et al., 2022), which is very important because scoring and ranking strongly influence the docking outcomes (Vittorio et al., 2024). Hence, we selected the models of low energy scores displaying the best ligand poses, as explained by other authors (Bhakat et al., 2018), to ensure the thermodynamic stability of the complexes. On the other hand, CABS-dock defines the medoids of the top models using different clustering protocols, and provides model 1 as the

Table 2
The PRODIGY interaction analysis and energy profiles of NSP1-Pln-JK and NSP1-PEP5 docked complexes.

Contact and energy profile		NSP1-Pln-JK complex		NSP1-PEP5 complex	
Class	Type	PatchMan	CABS-dock	PatchMan	CABS-dock
ICs (Number)	Charged-charged	14	15	1	7
	Charged-polar	11	14	6	6
	Charged-apolar	19	28	8	11
	Polar-polar	0	1	2	3
	Polar-apolar	11	9	14	8
	Apolar-apolar	19	20	13	14
NIS (%)	Charged	33.04	33.94	31.63	27.43
	Apolar	42.86	44.04	42.86	49.56
Energy profile					
Binding affinity (kcal/mol)		9.1	9.1	−7.2	−5.9
K_D (M)		2.1×10^{-7}	2.1×10^{-7}	4.8×10^{-6}	4.8×10^{-5}

K_D: dissociation constant; PEP5: peptide 5; Pln-JK: plantaricin JK; NSP1: non-structural protein-1 of SARS-CoV-2.

most representative of the best cluster (Kurcinski et al., 2015), this is as represented in Fig. S3 and Fig. S4.

Molecular docking provides the binding affinity between a target protein and ligand (small molecule or peptide) in computational drug discovery by predicting binding energy (Bhardwaj et al., 2021; Sharma et al., 2021b; Mandal and Mandal, 2024a), and the lower the binding energy the higher the binding affinity. Higher binding affinity thus defines the tighter binding of a ligand to a protein exhibiting stronger intermolecular (protein-ligand) interaction (Mandal and Mandal, 2024a, 2024b). Thus, molecular docking outputs help to justify the ligand's fitness to the binding site (involving various amino acid residues as explained below) of receptor proteins selecting the active most molecule with its best docking pose (Mandal and Mandal, 2024c), and the favourable docking, on the other hand, help verify how much a computational biology tool is efficient to perform molecular docking. Therefore, in the current study, molecular docking results demonstrate Pln-JK as a suitable drug candidate to combat SARS-CoV-2 infection by targeting the NSP1 protein.

3.3. PRODIGY analysis of protein-peptide complexes

The PRODIGY interaction analysis and energy profiles of NSP1-Pln-JK and NSP1-PEP5 complexes are represented in Table 2. The NSP1-Pln-JK docked complexes obtained from PatchMAN as well as CABS-dock displayed a binding affinity of −9.1 kcal/mol, while the K_D value (dissociation constant) for both the complexes (PatchMAN and CABS-dock-generated) was 2.1×10^{-7} (Table 2). The NSP1-PEP5 had binding affinity of −7.2 (for PatchMAN complex) and −5.9 kcal/mol (for CABS-dock complex), while the K_D values were 4.8×10^{-6} and 4.8×10^{-5} M for PatchMAN-derived complex and CABS-dock-derived complex, respectively (Table 2). Thus, using PRODIGY, it has been confirmed that the PatchMAN-derived NSP1-PEP5 complex displayed stronger affinity between NSP1 and PEP5 than the CABS-dock-derived complex, whereas both NSP1-Pln-JK (PatchMAN and CABS-dock-generated) complexes had similar binding affinities between NSP1 and Pln-JK. These results indicate the robustness of the PRODIGY tool to cross-check PatchMAN and CABS-dock docking results, although discrepancies were found between the findings of PatchMAN and CABS-dock complexes (in terms of both binding affinity and K_D values) for the NSP1-PEP5 complex, whereas concordance was observed for the NSP1-Pln-JK complex. However, PRODIGY analysis for PatchMAN and CABS-dock-generated complexes confirmed once again that Pln-JK had

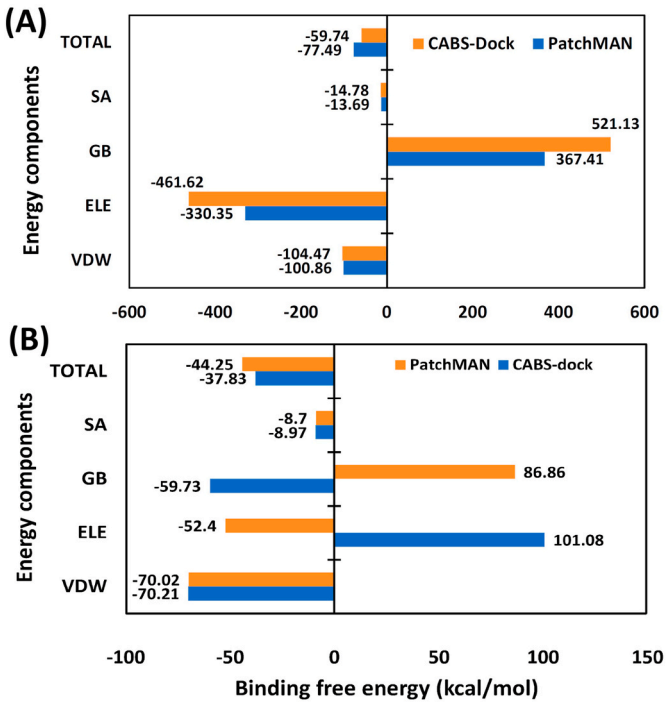

Fig. 4. Hawk-Dock-based MM-GBSA binding free energy profiles (A) NSP1-Pln-JK complexes generated from PatchMan and CABS-Dock. (B) NSP1-PEP5 complexes generated from PatchMan and CABS-Dock. VDW: van Der Waals interaction energy; ELE: Electrostatic energy; GB: Generalized Born model for polar solvation free energy estimation; SA: surface area for nonpolar solvation free energy estimation.

a greater affinity for the NSP1 protein of SARS-CoV-2 than the reference inhibitor PEP5. Various intermolecular contacts (ICs) as well as charged and apolar amino acids on the non-interacting surface (NIS) are shown in Table 2. The SARS-CoV-2 spike glycoprotein receptor-binding domain (RBD) inhibition property of designed peptides has previously been reported with binding energies −8.0 to −4.6 kcal/mol (Ramirez-Acosta et al., 2022). Demonstration of SARS-CoV-2 RBD inhibition has been made by small peptides using different docking tools, including HawDock docking displaying the binding free energy from −37.2 kcal/mol to −28.15 kcal/mol (Biswas et al., 2022), while PLpro of SARS-CoV-2 inhibition with gramicidin D has been demonstrated with −6.9 kcal/mol binding energy by molecular docking (Protić et al., 2023). The bacteriocins, pediocin PA-1 and salivaricin P, from lactic acid bacteria had docking score of −12 kcal/mol against SARS-CoV-2 RBD, as predicted through PRODIGY (Erol et al., 2023).

The PRODIGY webserver predicts binding energies as well as K_D values for protein-peptide complexes ascertaining the efficacy of peptide inhibitors, as this web-tool provides information comparable to experimental results in terms of quality and accuracy (Ramirez-Acosta et al., 2022). In the current study, we determined binding affinity and K_D values, and analysed residue interaction maps to show the inhibitory action of Pln-JK, a bacteriocin AMP, and PEP5, a reference antiviral peptide, against NSP1 of SARS-CoV-2. The fruit bromelain, a large peptide extractable from pineapple (*Ananas comosus*), exhibited K_D values ranging from 3.7^{-12} M to 1.1^{-11} M, and binding affinity from −15.6 kcal/mol to −14.9 kcal/mol against SARS-CoV-2 RBD (Tallei et al., 2021). Ramirez-Acosta et al. (2022) used PRODIGY to predict SARS-CoV-2 RBD inhibition by various AMPs, which demonstrated stronger inhibitory activity than the ACE-2-derived antiviral peptide. Similarly, in the current study, Pln-JK was more active than PEP5, in terms of binding affinity and K_D values predicted against NSP1 target protein (Table 2).

Calculating the K_D in the binding between a protein and a peptide

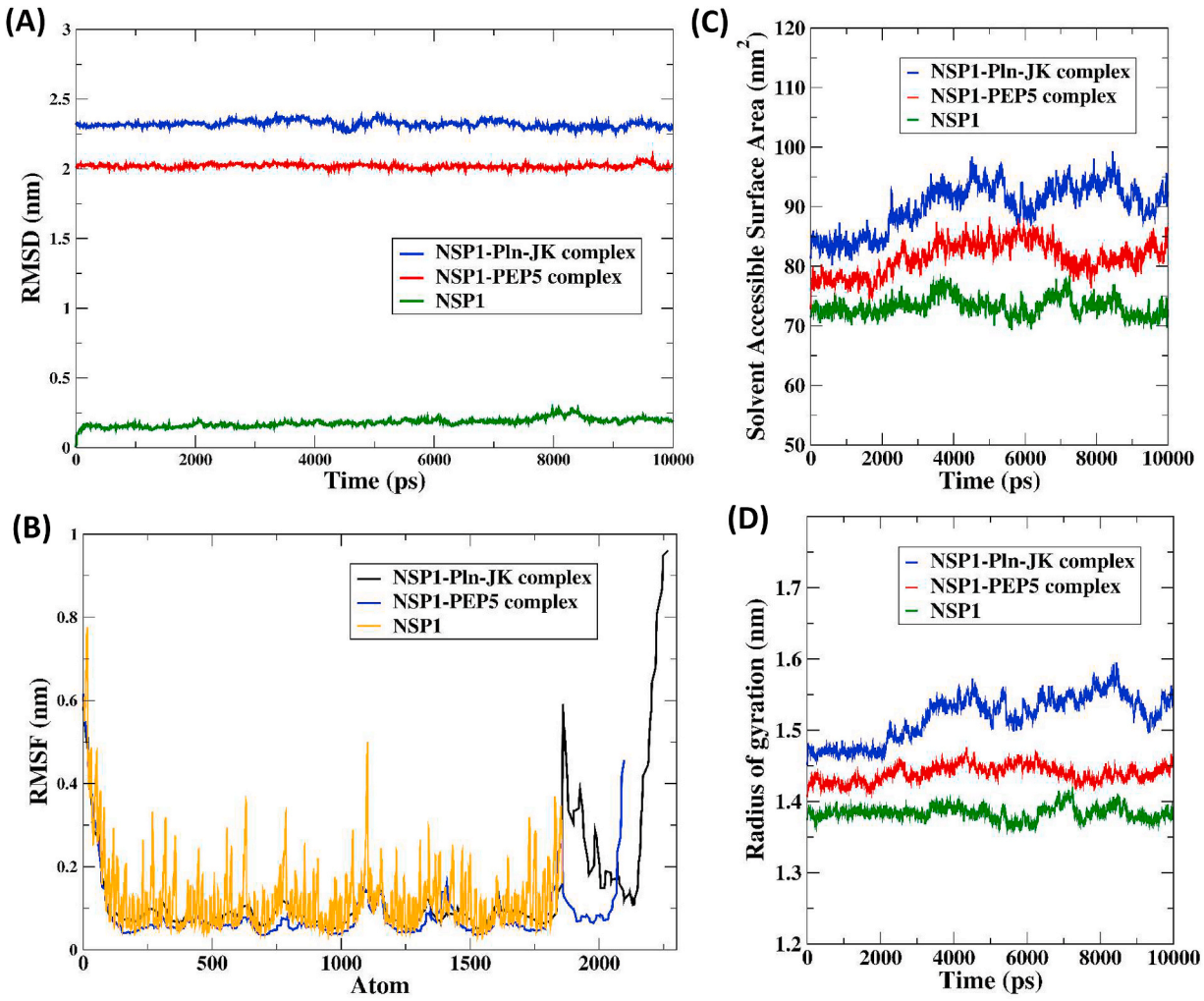

Fig. 5. The MDS profiles for NSP1-Pln-JK complex compared to NSP1-PEP5 complex. (A) RMSD (B) RMSF (C) SASA (D) Rg plots of NSP1 and NSP1-ligand (Pln-JK/PEP5) complexes. MDS, molecular dynamics simulation; RMSD, root mean square deviation; RMSF, root mean square fluctuation; SASA, solvent-accessible surface area; Rg, radius of gyration.

ligand is crucial in structure-based peptide drug discovery (Mandal and Mandal, 2024a), because it measures the binding affinity (in terms of binding energy) between the two, and the lower the K_D values the lower the binding energies, which signifies stronger affinity of the peptide to the target protein for successful binding. Notably, a higher K_D signifies weaker affinity, and as such the ligands show weaker or less strong binding to the protein (Tallei et al., 2021). In the current study, Pln-JK had lower K_D (2.1×10^{-7}) as well as binding energy (9.1 kcal/mol) compared to the reference antiviral peptide, PEP5 (binding energy: 7.2 kcal/mol for PatchMan complex and −5.9 kcal/mol for CABS-dock complex; K_D: 4.8×10^{-6} M for PatchMan complex and 4.8×10^{-5} M for CABS-dock complex), and thus, Pln-JK has been confirmed as a more active NSP1 inhibitor than PEP5.

3.4. HawkDock-based MM-GBSA binding free energy

Binding free energy calculation is crucial to predict the energetic stability of protein-peptide docked complex (Mandal and Mandal, 2024a; Erol et al., 2023). In the current study, the MM-GBSA binding free energy, as estimated using HawkDock webserver, for the PatchMAN-generated NSP1-Pln-JK docked complex was −77.49 kcal/mol (Fig. 4), wherein the energy break-up was: VDW (−100.86 kcal/mol), ELE (−330.35 kcal/mol), GB (367.41 kcal/mol) and SA (−13.69 kcal/mol). The MM-GBSA free energy as achieved for the CABS-dock-generated NSP1-Pln-JK docked complex was −59.74 kcal/mol, with energy break-up of VDW (−104.47 kcal/mol), ELE (−461.62 kcal/mol), GB (521.13 kcal/mol) and SA (−14.78 kcal/mol) (Fig. 4).

The MM-GBSA binding free energy for NSP1-PEP5 complexes are represented in Fig. 4; the PatchMAN-derived and CABS-dock-derived complexes had the values of −44.25 kcal/mol and −37.83 kcal/mol, respectively. This helps to understand that PEP5 successfully binds to NSP1, although Pln-JK showed a greater affinity for NSP1 as justified by the lower (MM-GBSA-based) binding free energies of the NSP1-Pln-JK complexes (Fig. 4). Moreover, it is also justified that PatchMAN demonstrated stronger binding between NSP1 and both Pln-JK and PEP5, when compared with the CABS-dock-generated complexes (NSP1-Pln-JK and NSP1-PEP5). Such inconsistency of results (in terms of binding free energy) reveals that PatchMAN performs more reliable docking by generating high quality models (protein-peptide complexes), which has also been proven using Ramachandran plot analysis (Figs. 2 and 3). The bacteriocins, such as pediocin PA-1, salivaricin P and salivaricin B exhibited inhibitory efficacy against RBD of SARS-CoV-2 spike protein, as demonstrated using MM-GBSA energies, which ranged from −132.68 kcal/mol to −109.63 kcal/mol (Erol et al., 2023). The MM-GBSA-based binding free energy has previously been calculated for protein-peptide complex using HawDock webserver (Mandal and Mandal, 2024a; Biswas et al., 2022).

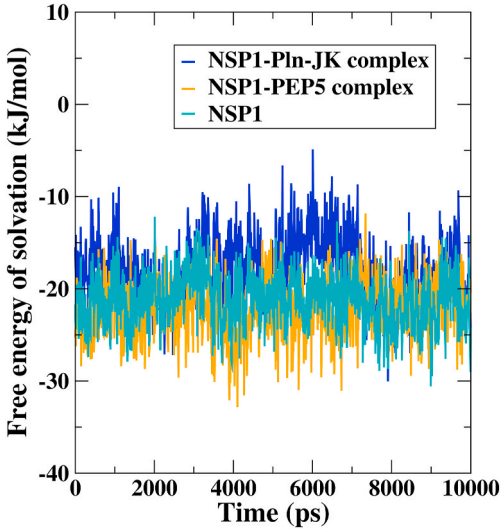

Fig. 6. Free energy of solvation of NSP1 and NSP1-ligand (Pln-JK/PEP5) complexes.

3.5. Molecular dynamics simulation and MM-PBSA binding free energy

As explained by the earlier authors for SARS-CoV-2 target protein-small molecular weight inhibitor complexes (Singh et al., 2021b; Chowdhury and Bagchi, 2022; Mandal and Mandal, 2021), herein, we performed MDS and post-MDS analysis was done by MM-PBSA binding free energy calculations for the NSP1-Pln-JK and NSP1-PEP5 complexes derived from PatchMAN docking to know their dynamic behaviour and energetic stability. We used different metrics to measure, such as RMSD, RMSF, SASA and Rg (Fig. 5). RMSD measures protein stability by depicting the deviation of protein backbone atoms, RMSF provides knowledge of residue level fluctuations (flexibility), SASA defines the protein's surface area exposed to the solvent, justifying structural stability, while Rg measures the overall compactness of the protein (Mahmud et al., 2021; Mandal and Mandal, 2024b).

The RMSD values, as shown in Fig. 5A, ranged 0.0005–0.281 (average: 0.18 ± 0.09 nm), 2.25–2.38 (average: 2.32 ± 0.02 nm) and 1.97–2.07 (average: 2.02 ± 0.01 nm) for NSP1, NSP1-Pln-JK and NSP1-PEP5, respectively, while the RMSF values were 0.034–0.77 (average: 0.12 ± 0.09 nm), 0.047–0.96 (average: 0.13 ± 0.13 nm) and 0.035–0.61 (average: 0.08 ± 0.07 nm), respectively (Fig. 5B). The RMSD profiles indicated the stability of the molecules throughout the simulation period, although the values were slightly higher for protein-peptide complexes these had similar pattern (Fig. 5A). Both complexes (NSP1-Pln-JK and NSP1-PEP5) exhibited similar fluctuation patterns, where the complexes had higher fluctuations than the NSP1 target for some residues (Fig. 5B), due to their involvement in interactions with the ligands (Pln-JK and PEP5) during complex formation. The average SASA values of NSP1, NSP1-Pln-JK and NSP1-PEP5 were73.23 ± 1.63, 90.17 ± 3.99 and 81.51 ± 2.75 nm^2, respectively (Fig. 5C), and Rg values were 1.30 ± 0.009, 1.51 ± 0.031 and 1.43 ± 0.011 nm, respectively (Fig. 5D), which further justified the stability of the complexes as well as their compactness and folding ability.

Additionally, we determined the free energy of solvation (Fig. 6), which in drug discovery is a prerequisite for protein-ligand complexation, and contributes to binding affinity (Choi et al., 2013). The solvation free energy influences the solubility of a drug in biological solvents, thereby defining its bioavailability and bioactivity, and helps identify the effective drug candidates with favourable physicochemical properties. We previously showed the free energy of salvation of the plant-derived small molecule ligands L-hyoscyamine (−34.97 ± 0.41 kJ/mol), eupatorium (−34.29 ± 0.38 kJ/mol) and alkaloid L27 from *Lycopodium* (−35.98 ± 0.44 kJ/mol) that interacted with SARS-CoV-2 3CLpro (3-chymotrypsin-like protease), demonstrating favourable binding between protein and ligands (Mandal and Mandal, 2021). In our present study, the free energies of salvation for NSP1-Pln-JK (−10.0008 ± 3.81 kJ/mol), NSP1-PEP5 (−22.28 ± 3.17 kJ/mol) and NSP1 (−21.15 ± 2.90 kJ/mol) (Fig. 6), specify the solubility and possible binding affinity of the molecules.

Table 3
MM-PBSA-based binding free energy for Pln-JK and PEP5 against NSP1 protein by MDS analysis.

Energy component (kcal/mol)	ΔG(MM-PBSA) ± SE	
	NSP1-Pln-JK	NSP1-PEP5
ΔVDWAALS	−42.46 ± 0.66	−39.64 ± 0.56
ΔEEL	−336.62 ± 4.58	−84.09 ± 3.42
ΔEPB	353.88 ± 3.97	104.38 ± 3.24
ΔENPOLAR	−6.69 ± 0.06	−5.59 ± 0.06
ΔGGAS	379.08 ± 4.49	−123.73 ± 3.32
ΔGSOLV	347.19 ± 3.96	98.79 ± 3.22
ΔTOTAL	−31.89 ± 0.91	−24.94 ± 0.6

ΔTOTAL: total binding free energy; ΔVDWAALS: van der Waals energy; ΔEEL: electrostatic energy; ΔEPB: polar solvation energy in Poisson–Boltzmann method; ΔENPOLAR: nonpolar solvation energy in Poisson–Boltzmann method; ΔGGAS: gas-phase molecular mechanics free energy; ΔGSOLV: solvation free energy; MM-PBSA: Molecular mechanics/Poisson-Boltzmann surface area; PEP5: peptide 5; Pln-JK: plantaricin JK; NSP1: non-structural protein-1 of SARS-CoV-2.

Many plant-derived bioactive compounds, such as oolonghomobisflavan-A, theasinensin-D, barrigenol, kaempferol, myricetin, curcuminoids, diacetylcurcumin and dicaffeoylquinic acid (Bhardwaj et al., 2021; Singh et al., 2021b, 2022; Sharma et al., 2021b) and AMPs including glycocin F, lactococcine G, Plantaricin NC8 αβ and bromelain (Balmeh et al., 2021; Omer et al., 2022; Tallei et al., 2021), have shown the capacity to inhibit various SARS-CoV-2 targets (3CLpro (Mpro), NSP15, spike protein RBD, RdRp, S protein, and N proteins), as demonstrated using MM-PBSA energy calculations following MDS studies. In the present study, we calculated MM-PBSA-based binding free energies for the PatchMan-generated NSP1-Pln-JK and NSP1-PEP5 complexes (Table 3), as these exhibited stronger binding affinities by MM-GBSA analysis (Fig. 4).

The MM-PBSA approach, which accurately demonstrates the binding stability of protein-ligand interactions, is vital for justifying drug efficacy against disease targets, where lower binding free energy implies stronger binding (Mandal and Mandal, 2024b; Singh et al., 2021b; Sharma et al., 2021b). In our study, NSP1-Pln-JK and NSP1-PEP5 had MM-PBSA binding free energies of −31.89 ± 0.91 and −24.94 ± 0.6 kcal/mol, respectively (Table 3). It was found that electrostatic energy (−336.62 ± 4.58 kcal/mol), van der Waals energy (−42.46 ± 0.66 kcal/mol) and nonpolar solvation energy (−6.69 ± 0.06 kcal/mol) contributed to a total energy of −31.89 ± 0.91 kcal/mol for the NSP1-PEP5 complex. In the case of NSP1-PEP5 complex, the gas-phase molecular mechanics free energy (−123.73 ± 3.32 kcal/mol), electrostatic energy (−84.09 ± 3.42 kcal/mol), van der Waals energy (−39.64 ± 0.56 kcal/mol) and nonpolar solvation energy (−5.59 ± 0.06 kcal/mol) played important roles in achieving a total binding free energy of −24.94 ± 0.6 kcal/mol. The van der Waals energy, or both electrostatic and van der Waals energies, were the main driving forces in protein-ligand interactions, as reported by the previous authors (Singh et al., 2021b; Sharma et al., 2021b), who confirmed anti-SARS-CoV-2 activities of barrigenol (−76.073 kJ/mol), kaempferol (−66.259 kJ/mol) and myricetin (−65.663 kJ/mol) by targeting NSP15 protein, and of dicaffeoylquinic acid (−193.74 kJ/mol) by targeting S-RBD, using MM-PBSA analysis. Thus, as explained before (Genheden and Ryde, 2015; Mandal and Mandal, 2024b), herein MM-PBSA, along with MM-GBSA, binding free energy calculations validate the energetic stability of the protein-ligand complexes (NSP1-Pln-JK and NSP1-PEP5 in our study) formed during molecular docking. Furthermore, echoing the

Table 4
Hawk-Dock docking analysis of NSP1-Pln-JK complex for energy contribution of top ten amino acid residues of NSP1 receptor protein and Pln-JK bacteriocin (ligand).

NSP1-Pln-JK complex	Residue	Energy components (kcal/mol)					Residue	Energy components (kcal/mol)				
	Receptor	VDW	ELE	GB	SA	TOTAL	Ligand	VDW	ELE	GB	SA	TOTAL
CABS-generated	Arg99	−4.57	−17.34	17.56	−0.83	−5.18	Trp3	−6.16	0.29	0.79	−0.86	−5.94
	Leu61	−3.37	−1.98	2.69	−0.49	−3.15	Ile23	−4.49	0.47	−0.17	−0.92	−5.12
	Tyr97	−3.54	−0.23	1.62	−0.67	−2.82	Phe6	−5.09	−0.76	2.05	−0.82	−4.62
	Leu39	−2.63	2.01	−1.75	−0.36	−2.73	Tyr15	−5.5	−1.49	3.81	−0.92	−4.09
	Lys58	−0.21	5.61	−7.69	−0.27	−2.56	Ala22	−2.53	−8.89	8.14	−0.45	−3.74
	Ser100	−2.22	2.88	−2.63	−0.24	−2.21	Ser8	−0.25	−9.68	6.79	−0.29	−3.43
	Glu93	−1.8	−47.86	48.22	−0.35	−1.79	Ser9	−0.69	−6.7	4.51	−0.29	−3.17
	Leu88	−2.64	1.61	−0.08	−0.35	−1.46	Phe14	−2.89	−4.26	4.36	−0.33	−3.12
	Gly101	−1.48	−1.53	1.87	−0.27	−1.41	Asn5	−5.05	0	2.93	−0.7	−2.82
	Ser40	−1.53	0.08	0.38	−0.19	−1.26	Arg24	−4.46	−60.84	63.6	−0.7	−2.41
PatchMAN-generated	Ile87	−3.48	−3.76	3.46	−0.4	−4.18	Arg142	−1.86	−32.21	28.9	−0.76	−5.93
	Arg116	−1.42	19.24	−21.5	−0.43	−4.12	Phe131	−4.62	−3.38	3.6	−0.65	−5.05
	Arg91	−3.2	8.32	−7.99	−0.8	−3.67	Leu127	−4.15	0.12	0.05	−0.57	−4.55
	Gln88	−4.29	−3.85	4.96	−0.48	−3.66	Gly134	−1.65	−10.93	9	−0.43	−4.01
	Leu53	−3.64	0.73	−0.02	−0.33	−3.26	Phe123	−4.11	−0.69	1.6	−0.47	−3.68
	Asp67	−0.08	−75.14	72.65	−0.28	−2.85	Ala119	−1.69	−3.78	2.52	−0.49	−3.44
	Gly86	−2.9	−2.42	3.04	−0.52	−2.8	Tyr132	−1.98	−6.47	5.97	−0.2	−2.68
	Glu94	−0.96	−105.92	104.6	−0.41	−2.69	Arg141	−6.06	−2.25	6.64	−0.94	−2.6
	Tyr89	−2.39	−2.01	2.13	−0.28	−2.55	Ser126	−4.65	−1.1	4.43	−0.65	−1.97
	Pro54	−1.75	0.4	−0.31	−0.25	−1.9	Glu135	−3.71	16.2	−13.85	−0.56	−1.92

VDW: Van Der Waals interaction energy; ELE: Electrostatic energy; GB: Generalized Born model for polar solvation free energy estimation; SA: surface area for nonpolar solvation free energy estimation; Pln-JK: plantaricin JK; NSP1: non-structural protein-1 of SARS-CoV-2.

Table 5
Hawk-Dock docking analysis of NSP1-PEP5 complex for energy contribution of top ten amino acid residues of NSP1 receptor protein and PEP5 reference antiviral peptide (ligand).

NSP1-PEP5 complex	Residue	Energy components (kcal/mol)					Residue	Energy components (kcal/mol)				
	Receptor	VDW	ELE	GB	SA	TOTAL	Ligand	VDW	ELE	GB	SA	TOTAL
CABS-generated	Arg124	−4.54	−88.07	86.86	−0.97	−6.72	Tyr11	−5.51	−4.06	4.25	−0.94	−6.25
	Leu39	−3.76	0.71	−0.15	−0.43	−3.63	Leu13	−3.87	−2.26	3.08	−0.71	−3.76
	Tyr97	−1.65	−3.68	2.32	−0.35	−3.36	Tyr2	−3.27	0.74	0	−0.52	−3.05
	Pro80	−2.58	−0.54	1.02	−0.4	−2.5	Ala3	−2.83	−3.8	4.67	−0.53	−2.5
	Arg99	−1.03	−38.3	37.42	−0.21	−2.12	Val14	−3.45	0.97	0.86	−0.57	−2.19
	Gly98	−0.91	−7.28	6.5	−0.13	−1.81	Asn7	−0.73	−6.22	5.13	−0.18	−2.01
	Met85	−1.38	−2.74	2.82	−0.37	−1.66	Asn12	−2.18	−0.8	2.72	−0.31	−0.57
	Leu88	−2.31	2.82	−1.75	−0.33	−1.56	Leu4	−0.83	1.55	−0.8	−0.15	−0.23
	Hie13	−1.99	2.63	−1.56	−0.26	−1.18	Ala8	−0.31	0.03	0.14	0	−0.14
	Val89	−0.99	−0.2	0.28	−0.02	−0.93	Asp10	−1.84	3.47	−1.49	−0.19	−0.06
PatchMAN-generated	Lys50	−1	−94.99	92.33	−0.43	−4.09	Leu121	−6.57	−2.12	3.16	−0.77	−6.31
	Val48	−4.35	−5.3	6.33	−0.43	−3.75	Tyr128	−5.68	−0.39	1.38	−0.73	−5.43
	Leu53	−3.49	−3.42	3.72	−0.31	−3.5	Leu122	−3.62	−0.28	0.4	−0.5	−3.99
	Glu94	−2.02	−12.86	13.15	−0.54	−2.27	Asn124	−3.43	−10.4	11.89	−0.52	−2.46
	Phe62	−1.48	−0.69	0.51	−0.12	−1.78	Ala125	−2.66	1.67	−1.11	−0.3	−2.4
	Thr95	−3.69	−5.64	8.09	−0.48	−1.72	Asn132	−3.7	30.8	−28.74	−0.6	−2.24
	Pro54	−1.46	−1.47	1.59	−0.26	−1.59	Asp127	−0.52	−28.13	28.22	−0.33	−0.77
	Gly86	−1.37	0.28	0.07	−0.29	−1.32	Asn129	−4.33	7.65	−3.29	−0.66	−0.62
	Gln58	−1.52	−4.2	4.93	−0.21	−1.01	Tyr119	−1	−0.08	0.67	−0.11	−0.51
	Glu49	−1.5	27.19	−26.43	−0.14	−0.89	Leu130	−0.53	1.6	−1.31	−0.09	−0.33

VDW: Van Der Waals interaction energy; ELE: Electrostatic energy; GB: Generalized Born model for polar solvation free energy estimation; SA: surface area for nonpolar solvation free energy estimation. NSP1: non-structural protein-1 of SARS-CoV-2; PEP5: peptide 5.

previous findings for SARS-CoV-2 inhibitors (Singh et al., 2021b; Sharma et al., 2021), it is clear that Pln-JK formed a more stable complex with NSP1 than NSP1-PEP5 complex.

3.6. Protein-peptide interaction and bond analysis

Determining active amino acid residues of both protein and peptide is critical to ligand binding with its best poses inside the receptor molecule (Mandal and Mandal, 2024a; Selvaraju et al., 2020). The top ten energy-contributing ligand- and receptor residues of NSP1-Pln-JK complex (both from PatchMAN and CABS-dock) are shown in Table 4, while Table 5 shows the top ten energy-contributing residue components of NSP1-PEP5 complex (derived both from PatchMAN and CABS-dock). Moreover, various bonds, interactions and contacts play a crucial role in protein-ligand binding (Ferreira De Freitas and Schapira, 2017; Panigrahi and Desiraju, 2007). The 2-D of NSP1-Pln-JK complex, based on PatchMAN and CABS-dock dockings, displayed a network of intermolecular interactions (hydrogen bond, salt bridge, and hydrophobic contacts), as analysed through DIMPLOT (Figs. 7 and 8). The PatchMAN-generated NSP1-Pln-JK complex displayed 10 hydrogen bonds with the involvement of seven residues, each of the NSP1 protein (chain A) (Glu94, Arg116, Asp67, Gly90, Arg91, Gln88, Gly86), and Pln-JK (chain B) bacteriocin residues: Gly118(2.76 Å), Ala119(2.79 Å), Arg142(2.66, 2.77, 2.94 Å), Glu135 (2.75, 3.05 Å), Gly134 (2.85 Å), Asp133 (3.02 Å) and Tyr132(3.12 Å), and one salt bridge (Fig. 7); the residues involved in the formation of hydrophobic contacts included 13 from NSP1 protein and seven from Pln-JK. In the case of the CABS-dock-generated complex, the NSP1 protein formed three hydrogen bonds employing Lys125, Lys58 and Glu87 residues with the respective Pln-JK residues Ser8 (2.80 Å), Arg25 (2.92 Å) and Ser9 (2.77

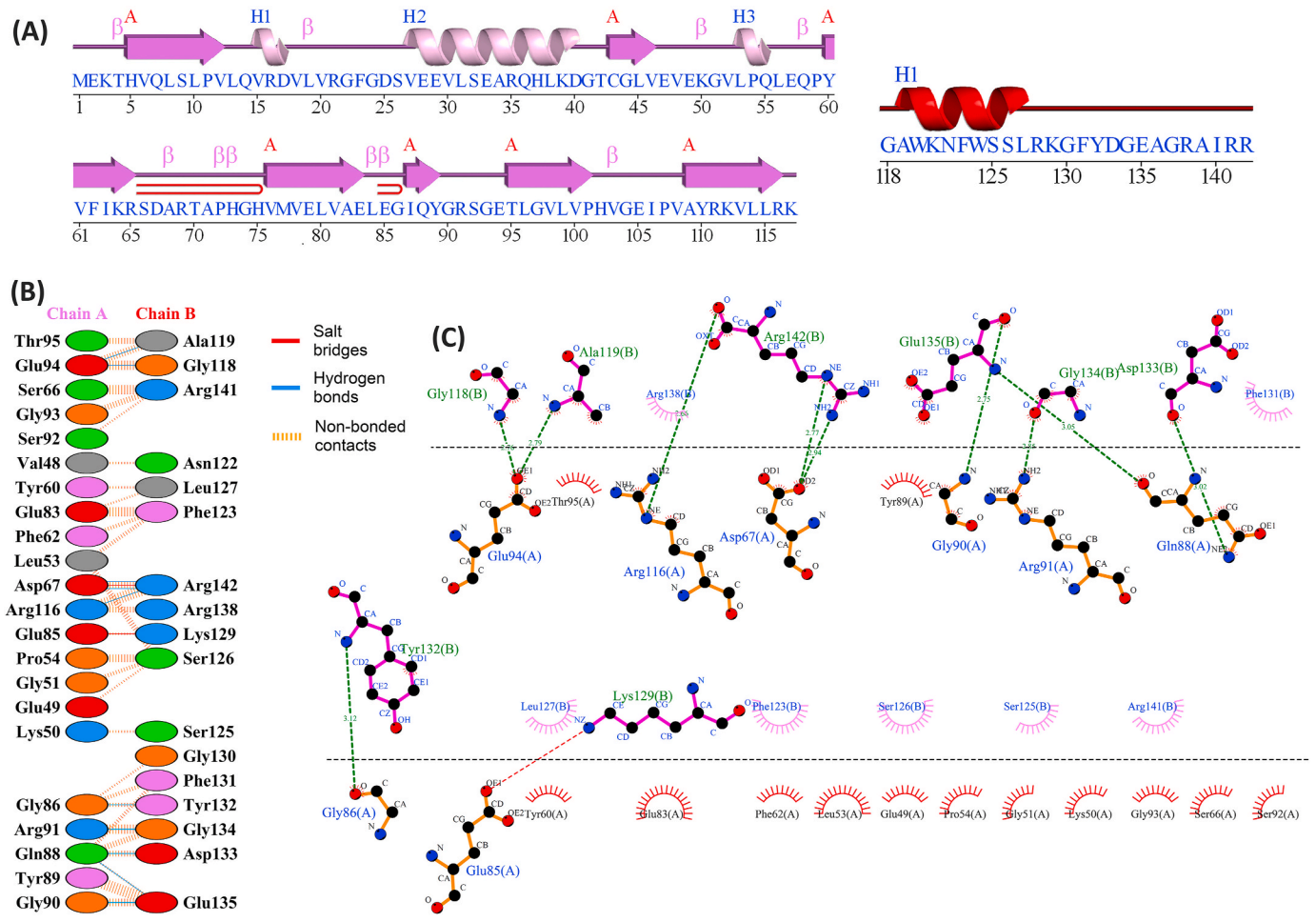

Fig. 7. Binding interaction of NSP1-Pln-JK complex generated from PatchMan (A) secondary structure of NSP1 (left 1 to 117 amino acid residues) and Pln-JK (right 118 to 142 amino acid residues) (B) Residue interaction map of NSP1-Pln-JK complex developed from PDB-sum generate displaying hydrogen bonds (blue lines), salt bridges (red lines) and nonbonded contacts (orange ticks) between NSP1 (chain A) and Pln-JK (chain B) residues at the interface. The colour depictions of amino acid residues of protein and bacteriocin are made with blue (basic), red (acidic), green (neutral), grey (aliphatic), pink (aromatic), orange (Pro&Gly) and yellow (cysteine) (C) The PRODIGY-based interaction of NSP1-Pln-JK complex exhibiting hydrogen bonds (green dot-lines), salt bridges (red dot-lines) and hydrophobic contacts (with amino acid residues of NSP1 in red arcs (chain A) and Pln-JK residues in pink arcs (B chain)). (For interpretation of the references to colour in this figure legend, the reader is referred to the Web version of this article.)

Å), respectively, along with the formation of two salt bridges (Fig. 8).

The 2-D representation of the NSP1-PEP5 complex, based on PatchMAN and CABS-dock dockings, displayed interactions exhibiting hydrogen bond and hydrophobic contacts, as analysed using DIMPLOT (Figs. 9 and 10). The PatchMAN-generated NSP1-PEP5 complex (Fig. 9) exhibited four hydrogen bonds using four residues of NSP1 protein (chain A: Glu94, Lys50, Val48, Glu83) as well as Pln-JK (chain B: Ile118 (2.74 Å), Asp127(2.40 Å), Asn124(3.23 Å), Asn132(3.15 Å), and there was a single salt bridge (Fig. 9B); the residues involved in the formation of hydrophobic contacts included 11 from NSP1 protein and six from PEP5. As shown in Fig. 10, the CABS-dock-generated NSP1-PEP5 complex displayed two hydrogen bonds involving Arg99 and Tyr97 from NSP1 protein (chain B), and Glu9 (3.02 Å) and Tyr11 (3.23 Å) from PEP5 (chain A). while the residues involved in the formation of hydrophobic contacts were 11 from NSP1 and seven from PEP5.

As shown in Table 4, for the CABS-dock-generated NSP1-Pln-JK complex, among the top 10 important energy-contributing amino acid residues involved in hydrogen bond formation included Arg99 and Lys58 of NSP1 and Ser8 and Ser9 of Pln-JK, whereas the residues displaying hydrophobic interactions were Leu61, Tyr97, Leu39, Ser100, Glu93, Leu88, Gly101 and Ser40 of NSP1, and Trp3, Ile23, Phe6, Tyr15, Ala22, Phe14, Asn5 and Arg24 of Pln-JK (Fig. 8). Similarly, in the case of PatchMan-derived NSP1-Pln-JK complex (Table 4), the top energy contributing hydrogen bond forming residues were Arg116, Arg91, Gln88, Asp67, Gly86 and Glu94 of NSP1, and Arg142, Gly134, Ala119, Tyr132 and Glu135 of Pln-JK, whereas the residues exhibiting hydrophobic interactions were Leu53 and Pro54 of NSP1, and Phe131, Leu127, Phe123, Arg141 and Ser126 of Pln-JK (Fig. 7). In the CABS-dock-generated NSP1-PEP5 complex (Fig. 10), Tyr97 and Arg99 (from NSP1) and Tyr11 (from PEP5) were top energy contributing residues (Table 5), which formed hydrogen bonds during intermolecular interactions, while the hydrophobic contacts were formed with the involvement of six (Arg124, Leu39, Gly98, Met85, Leu88, Val89) and five (Leu13, Ala3, Val14, Asn12, Asp10; from PEP5) top energy contributing residues from NSP1 and PEP5, respectively (Table 5). In the PatchMan-derived NSP1-PEP5 complex (Fig. 9), four top energy contributing residues (Lys50, Val48, Glu94, Gln58) from NSP1, and three (Asn124, Asn132, Asp127) from PEP5 formed hydrogen bonds, while Leu53, Phe62, Thr95, Pro54, Gly86 and Glu49 from NSP1, and Leu121, Tyr128, Leu122, Ala125, Asn129 and Tyr119 from PEP5 exhibited hydrophobic interactions (Table 5). Thus, a large number of amino acid residues from both Pln-JK and PEP5 have been shown to be important in generating different bonds for favourable interactions with different amino acid residues of the NSP1 target protein to successfully achieve binding with the best pose of the peptide ligand within the active binding site of the protein.

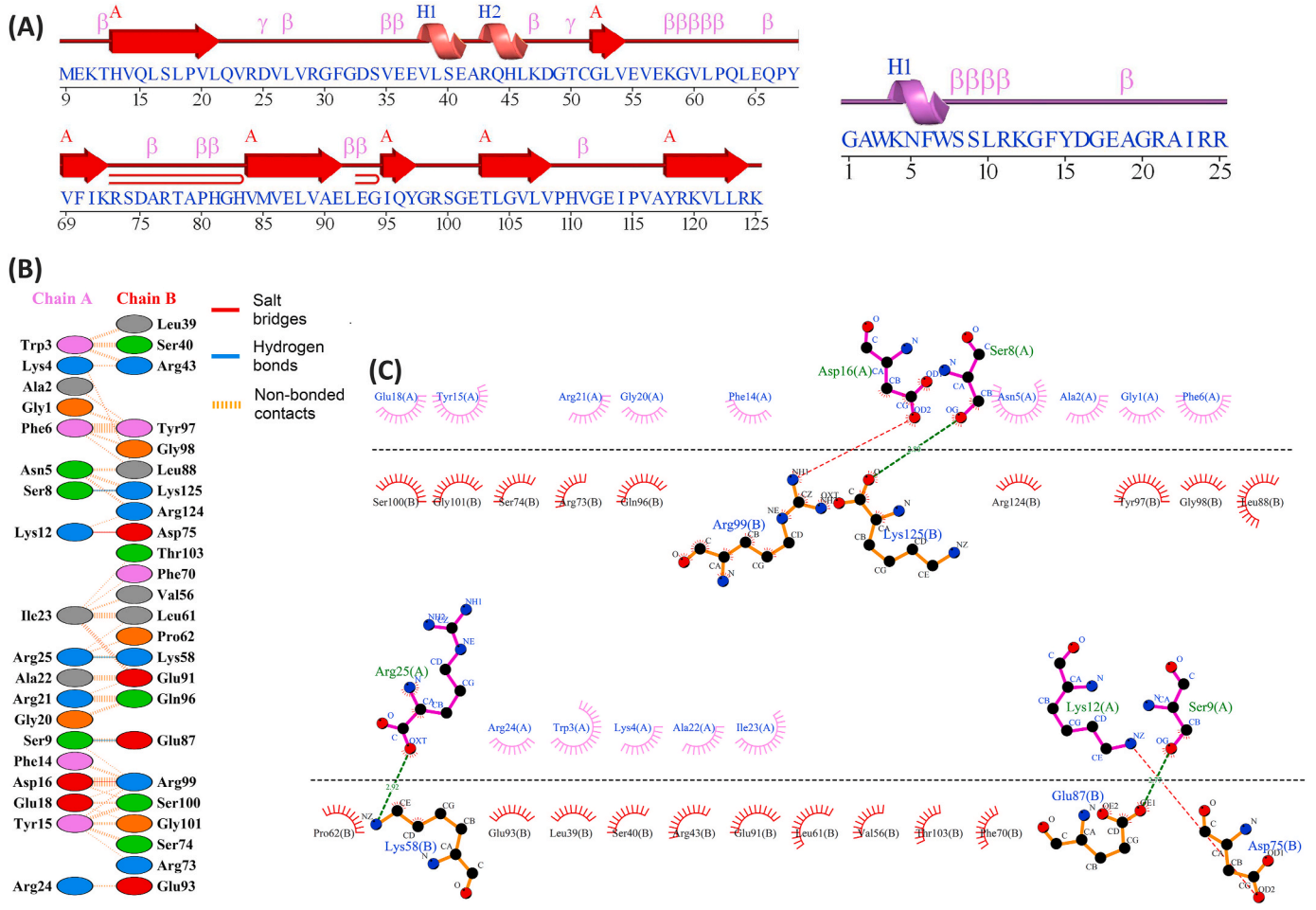

Fig. 8. Binding interaction of NSP1-Pln-JK complex generated from CABS-Dock (A) secondary structure of NSP1 (left, 117 amino acid residues: 9–125 residues) and Pln-JK (right 1 to 25 amino acid residues) (B) Residue interaction map of NSP1-Pln-JK complex developed from PDB-sum generate displaying hydrogen bonds (blue lines), salt bridges (red lines) and nonbonded contacts (orange ticks) between NSP1 (chain B) and Pln-JK (chain A) residues at the interface. The colour depictions of amino acid residues of protein and bacteriocin are made with blue (basic), red (acidic), green (neutral), grey (aliphatic), pink (aromatic), orange (Pro&Gly) and yellow (cysteine) (C) The PRODIGY-based interaction of NSP1-Pln-JK complex exhibiting hydrogen bonds (green dot-lines), salt bridges (red dot-lines) and hydrophobic contacts (with amino acid residues of NSP1 in red arcs (chain B) and Pln-JK residues in pink arcs (chain A)). (For interpretation of the references to colour in this figure legend, the reader is referred to the Web version of this article.)

Additionally, we analysed the thermodynamically more stable protein-peptide complexes (NSP1-Pln-JK and NSP1-PEP5) derived from PatchMan using BIOVIA to get more clear reflection on the interaction maps (Table S1 and Table S2). There were a total of 25 different interactions in the NSP1-Pln-JK complex (Table S1): salt bridges (n = 5), electrostatic (n = 3), conventional hydrogen bonds (n = 9), carbon hydrogen bonds (n = 6) and alkyl (n = 2). A total of 13 different interactions were demonstrated in the NSP1-PEP5 complex (Table S2), these are: salt bridges (n = 2), conventional hydrogen bonds (n = 2), carbon hydrogen bonds (n = 2), amide-π stacked (n = 1), alkyl (n = 3) and π-alkyl (n = 3). The amino acid residues and other parameters involved in the formation of various bonds, along with the hydrogen donors/acceptors, are tabulated (Table S1 and Table S2). Besides the salt bridges, a greater number of conventional hydrogen bonds, along with electrostatic interactions, were found in the case of NSP1-Pln-JK, for which the complex is stronger than the NSP1-PEP5 complex. The NSP1-Pln-JK/PEP5 complexes' secondary structures of the complex-forming molecules (NSP1 and Pln-JK), and interacting residue (at the protein-peptide interfaces) maps displaying hydrogen bonds, salt bridge and non-bonded contacts are shown in Figs. 7 and 8 (for NSP1-Pln-JK complexes) and in Figs. 7 and 8 (for NSP1-PEP5 complexes). The Ramachandran plots of the NSP1-Pln-JK and NSP1-PEP5 complexes, as displayed in Figs. 2 and 3, respectively, defined their (protein-peptide complex) structural authenticity (Agnihotry et al., 2022). The percentage of residues located in the most favoured regions of the Ramachandran plots explained this view (Figs. 2 and 3).

Omer et al. (2025) demonstrated the antiviral role of various two-peptide bacteriocins, including Pln-JK that showed envelop disrupting activity in Kunjin virus (KUNV). Pln-JK, a cationic (net charge +4) and amphiphilic bacteriocin, interacts with hydrophilic as well as hydrophobic amino acid residues of the receptor protein NSP1 (Fig. 7), by forming different bonds, and affirms its (Pln-JK) binding with the receptor (NSP1) within the specific site. This results in the inactivation of SARS-CoV-2 replication, and inhibition of host protein synthesis, immune dysfunction activities as well as the role of NSP1 in causing pathogenesis. Thus, by causing conformational changes in the metabolic and virulence enzyme NSP1, Pln-JK plausibly be effective in preventing SARS-CoV-2 infection.

During docking, intermolecular interactions occur through the formation of various bonds, which determine the receptor-ligand binding by achieving a binding energy. Strong binding of the ligand defines a strong inhibition of a protein associated with the pathogenesis of diseases, including COVID-19 (Bansal et al., 2021; Souza et al., 2020). As explained by earlier authors (Ciemny et al., 2018), in our study, peptide binding to the target protein was achieved through favourable interactions with various bond formations that alter the protein structure

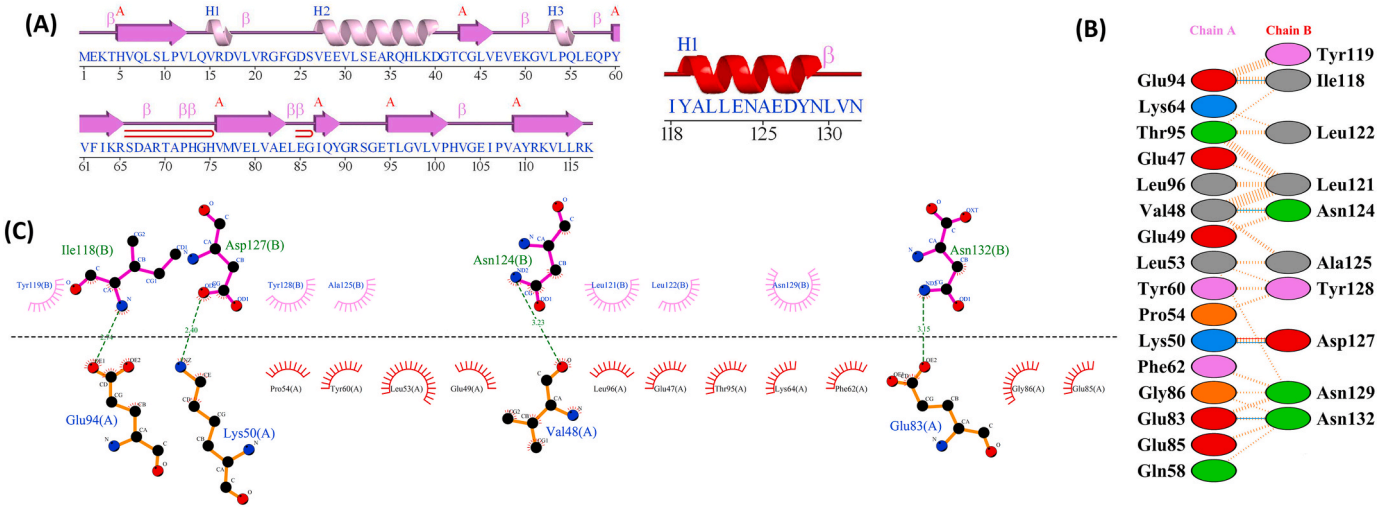

Fig. 9. Binding interaction of NSP1-PEP5 complex generated from PatchMan (A) secondary structure of NSP1 (left 1 to 117 amino acid residues) and PEP5 (right 118 to 132 amino acid residues) (B) Residue interaction map of NSP1-PEP5 complex developed from PDB-sum generate displaying hydrogen bonds (blue lines), salt bridges (red lines) and nonbonded contacts (orange ticks) between NSP1 (chain A) and PEP5 (chain B) residues at the interface. The colour depictions of amino acid residues of protein and peptide are made with blue (basic), red (acidic), green (neutral), grey (aliphatic), pink (aromatic) and orange (Pro&Gly) (C) The PRODIGY-based interaction of NSP1-PEP5 complex exhibiting hydrogen bonds (green dot-lines) and hydrophobic contacts (with amino acid residues of NSP1 in red arcs (chain A) and PEP5 residues in pink arcs (B chain)). (For interpretation of the references to colour in this figure legend, the reader is referred to the Web version of this article.)

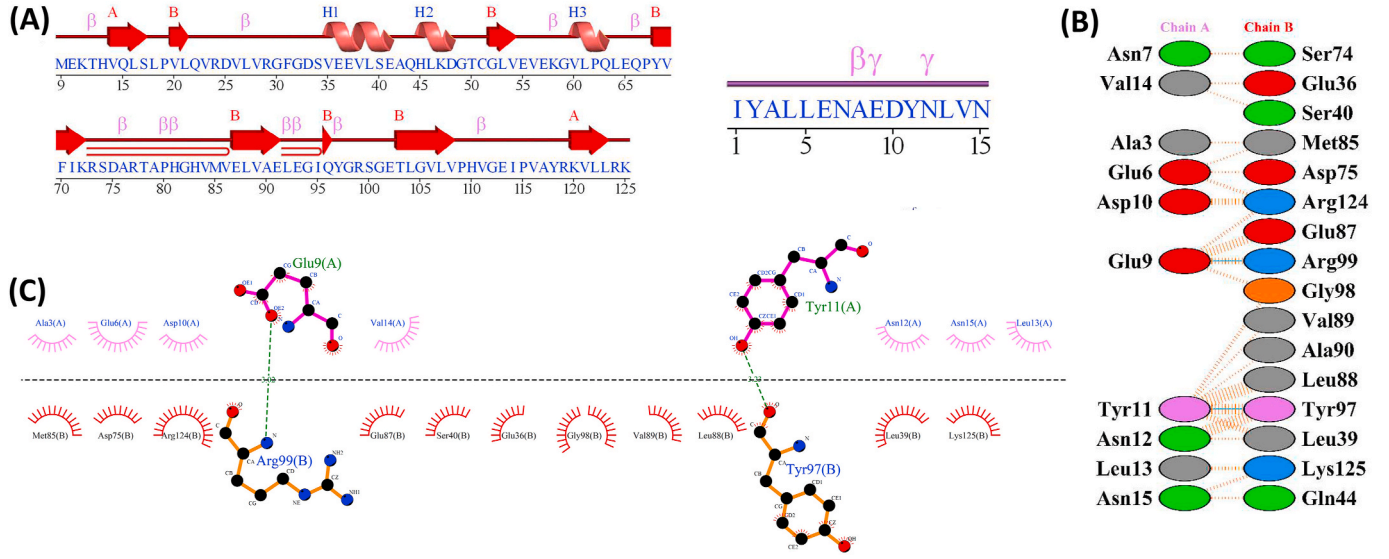

Fig. 10. Binding interaction of NSP1-PEP5 complex generated from CABS-Dock (A) secondary structure of NSP1 (left, 117 amino acid residues: 9–125 residues) and PEP5 (right 1 to 15 amino acid residues) (B) Residue interaction map of NSP1-PEP5 complex developed from PDB-sum generate displaying hydrogen bonds (blue lines) and nonbonded contacts (orange ticks) between NSP1 (chain B) and PEP5 (chain A) residues at the interface. The colour depictions of amino acid residues of protein and bacteriocin are made with blue (basic), red (acidic), green (neutral), grey (aliphatic), pink (aromatic) and orange (Pro&Gly) (C) The PRODIGY-based interaction of NSP1-PEP5 complex exhibiting hydrogen bonds (green dot-lines), salt bridges (red dot-lines) and hydrophobic contacts (with amino acid residues of NSP1 in red arcs (chain B) and PEP5 residues in pink arcs (chain A)). (For interpretation of the references to colour in this figure legend, the reader is referred to the Web version of this article.)

and its function. MDS results also support this view of the conformational changes of NSP1 upon peptide binding (Fig. 5). The key amino acid residues playing crucial roles in energy contributions and various bond formation in the NSP1-Pln-JK and NSP1-PEP5 complexes generated from both PatchMan and CABS-dock dockings are shown (Table S1 and Table S2). Additionally, the BIOVIA analysis of PatchMan-generated NSP1-Pln-JK and NSP1-PEP5 complexes, which were thermodynamically more stable than the CABS-dock generated complexes, revealed various bonds, including conventional hydrogen bonds, carbon hydrogen bonds, electrostatic bonds, salt bridges, and hydrophobic interactions (π-alkyl and alkyl) involving different amino acids (Table S1 and Table S2).

3.7. Peptide safety and toxicity analysis

Alongside the peptide activity, its safety profiling is an important step in computational drug discovery (Mandal and Mandal, 2024a; Rajpoot et al., 2022). Herein, the physicochemical properties of the bacteriocin Pln-JK and PEP5 reference antiviral, as determined through the PepCalc webserver, are shown in Figs. 11 and 12. The PEP5 has been

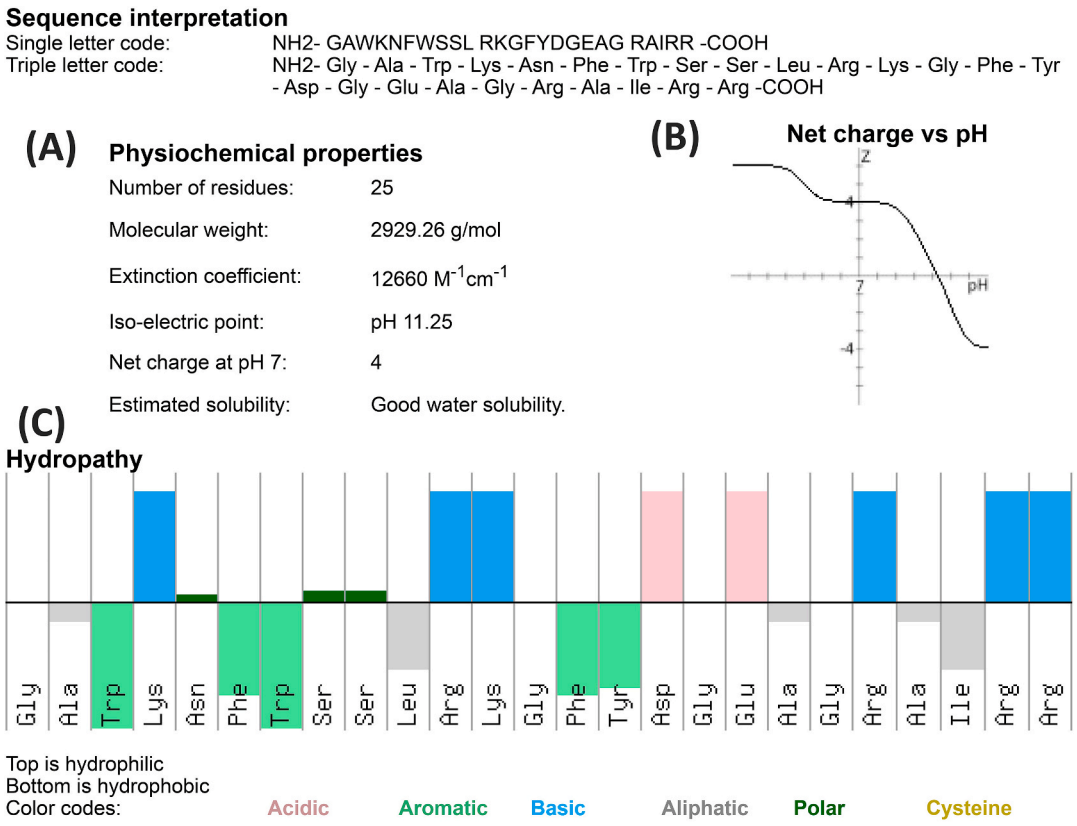

Fig. 11. PepCalc webserver derived (A) physicochemical characteristics (B) net charge versus pH plot (C) hydropathy features of Pln-JK bacteriocin.

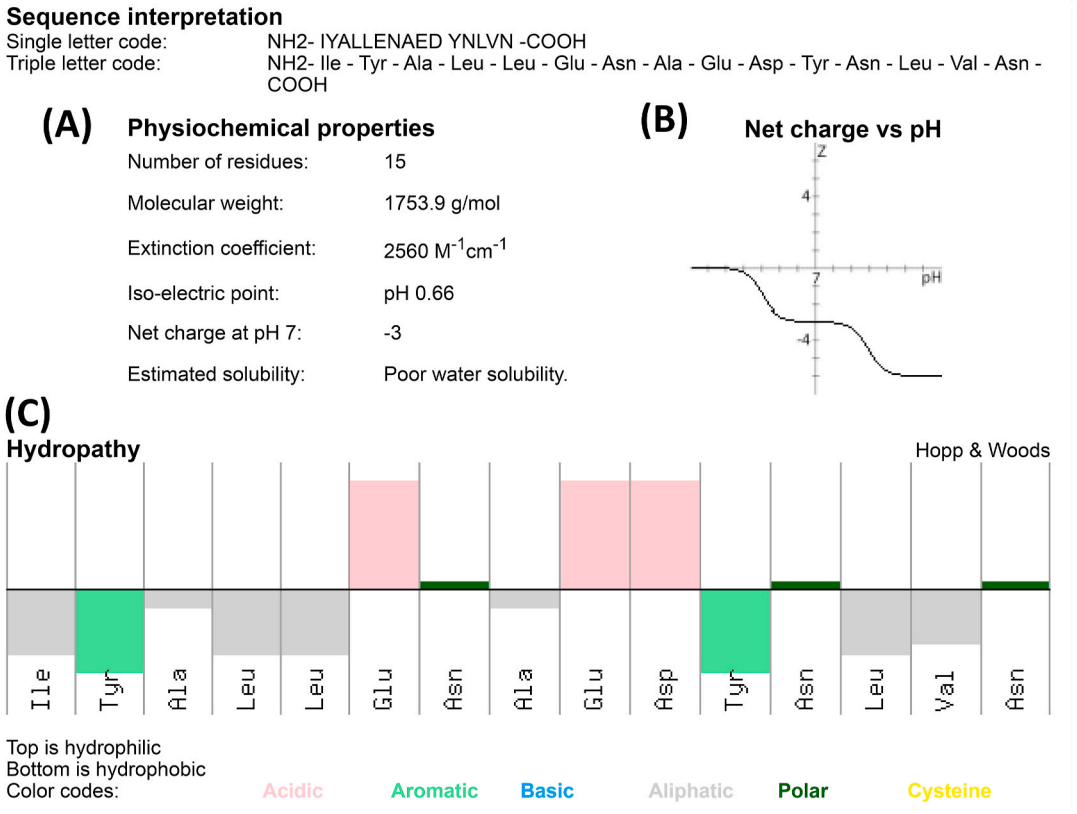

Fig. 12. PepCalc webserver derived (A) physicochemical characteristics (B) net charge versus pH plot (C) hydropathy features of PEP5 bacteriocin.

Table 6
Physicochemical properties, toxicity and allergenicity profiles of Pln-JK bacteriocin and reference antiviral peptide (PEP5).

Technique/ property	Pln-JK		PEP5	
	Occurrence	Prediction	Occurrence	Prediction
Prediction: machine learning (RF)[a]	ML score: 0.32	Non-allergen	ML score: 0.31	Non-allergen
IgE epitope mapping	No epitope found	Non-allergen	No epitope found	Non-allergen
Motif scan (model: MERCI)	No motifs found	Non-allergen	No motifs found	Non-allergen
BLAST search[b]	No Hits found	Non-allergen	No Hits found	Non-allergen
CSM-Toxin	Probability: 0.28	Non-toxic	Probability: 0.39	Non-toxic
ToxinPred	SVM score: 0.95	Non-toxin	SVM score: 1.12	Non-toxin
Stability	Probability: 92 %	Stable	Probability: 58 %	Unstable
Bioavailability	Score: 38.44 %	Low	Score: 40.78 %	Low

[a] Threshold value: 0.4.
[b] Followed allergen and non-allergen database. NSP1: non-structural protein-1 of SARS-CoV-2; Pln-JK: plantaricin JK; PEP5: peptide 5.

predicted to exhibit poor water solubility, while Pln-JK demonstrated good water solubility. Pln-JK and PEP5 showed a probability of 92 % (stable) and 58 % (unstable), respectively, while their oral bioavailability scores were 38.44 % and 40.78 %, respectively (Table 3). Both the bacteriocin and reference antiviral were tested, using AlgPred 2.0, as non-allergens (Table 3). The CSM-Toxin webtool detected Pln-JK and PEP5 as non-toxic, and the bacteriocin displayed an SVM score of −0.95 and PEP5 as −1.12 through ToxinPred, and thus predicted as non-toxin. The toxicity and allergenicity of the peptides intended to be future drugs have also been predicted by earlier authors (Jin et al., 2024).

Thus, the peptides have good efficacy and safety properties, making them good candidates for therapeutic applications. However, there are concerns about their *in vivo* instability, due to their biological hydrolysis as well as enzymatic degradation (Wang et al., 2022), which reduce the peptide's bioavailability (Han et al., 2019). This in turn limits the application of bioactive peptides for therapeutic usage (Udenigwe and Fogliano, 2017). In the current study, the physical and chemical stability and bioavailability of the bacteriocin peptide Pln-JK, derived from probiotic bacteria, were comparable (or in some facts better) to the synthetic reference antiviral PEP5 (Table 6). Overall, it has been reported that synthetic modifications including cyclization, lipidization and nano-formulations, can improve the systemic stability and bioavailability of peptides, restoring their therapeutic efficiency (Bruno et al., 2013).

3.8. Limitations and future direction of the study

The current study has some limitations: first, this computational study cannot recommend Pln-JK as a prescription drug for COVID-19 patients; second, to further confirm the inhibitory efficacy of Pln-JK, its binding to SARS-CoV-2 NSP1 is required to determine with high precision computational studies using QM/MM (quantum mechanics/molecular mechanics) simulations; third, this peptide inhibitor (Pln-JK) is required to be tested against various druggable targets from SARS-CoV-2 to check its multiple inhibitory actions; fourth, the efficacy and safety (pharmacokinetics and toxicity) of Pln-JK need to be validated using experimental evidences.

The current computational biology research is promising in shaping the future direction of development of therapeutic peptides, such as bacteriocins, which are naturally produced, especially by probiotic bacteria, subject to *in vitro* and *in vivo* experiments, and thereafter the necessary clinical trials. This can ensure the safety and efficacy, alongside the stability and bioavailability, of peptide therapy. Before that the application of more advanced *in silico* methods could improve peptide bioavailability and stability to prepare more effective bacteriocin peptides as real-time personalized therapy. Consequently, the current computationally predicted information may be translated into preclinical as well as clinical investigations for the therapeutic application of bacterially synthesized bacteriocins in the fight against SARS-CoV-2 infection.

4. Conclusion

In the current study, we utilized Pln-JK bacteriocin derived from *L. plantarum* as an inhibitor of SARS-CoV-2 NSP1. The molecular docking results revealed favourable binding of Pln-JK to NSP1 through the formation of a network of hydrogen bonds, hydrophobic interactions and salt bridges. The K_D values of 2.1×10^{-7} M and binding energy of 9.1 kcal/mol confirmed a good affinity between NSP1 and Pln-JK, as predicted by PRODIGY analysis. Additionally, by the MM-GBSA method, the very low binding free energy for the NSP1-Pln-JK complex, generated from both CABS-dock (−59.74 kcal/mol) and PatchMAN (−77.49 kcal/mol), confirmed the favourable binding affinity between NSP1 and Pln-JK. Finally, MM-PBSA-based binding free energy calculation for the NSP1-Pln-JK complex (−31.89 ± 0.91 kcal/mol) explained its energetic stability. On the other hand, NSP1-PEP5 complex exhibited higher binding free energy values by both MM-GBSA (−44.25 kcal/mol for PatchMAN complex; −37.83 kcal/mol for CABS-dock complex) and MM-PBSA (−24.94 ± 0.6 kcal/mol) methods. Thus, Pln-JK formed a thermodynamically more stable complex with NSP1 than the NSP1-PEP5 complex. Moreover, the Pln-JK bacteriocin was predicted as a water-soluble, non-allergic and non-toxic peptide. Overall, this computational study demonstrates a novel way to develop peptide-based drugs targeting SARS-CoV-2 NSP1, and herein Pln-JK has been established as a safe and effective drug candidate for SARS-CoV-2 infection. However, wet-lab research is mandatory to validate the current findings before using Pln-JK as a prescription drug.

CRediT authorship contribution statement

Manisha Mandal: Visualization, Software, Methodology, Conceptualization, Writing – review & editing. **Shyamapada Mandal:** Writing – review & editing, Validation, Supervision, Software, Methodology, Conceptualization, Visualization, Writing – original draft.

Funding information

The authors did not receive any funding for the current research.

Declaration of competing interest

The authors declare that they have no known competing financial interests or personal relationships that could have appeared to influence the work reported in this paper.

Appendix A. Supplementary data

Supplementary data to this article can be found online at https://doi.org/10.1016/j.amolm.2025.100080.

References

Abdulhussain, K.R., Razavi, S.H., 2020. Plantaricin bacteriocins: as safe alternative antimicrobial peptides in food preservation—a review. J. Food Saf. 40, e12735. https://doi.org/10.1111/jfs.12735.
Agnihotry, S., Pathak, R.K., Singh, D.B., Tiwari, A., Hussain, I., 2022. Protein structure prediction. In: Bioinformatics. Elsevier, pp. 177–188. https://doi.org/10.1016/B978-0-323-89775-4.00023-7.

Aljohani, A., Rashwan, N., Vasani, S., Alkhawashki, A., Wu, T.T., Lu, X., Castillo, D.A., Xiao, J., 2024. The health benefits of probiotic lactiplantibacillus plantarum: a systematic review and meta-analysis. Probiotics & Antimicro. Prot. https://doi.org/10.1007/s12602-024-10287-3.

Anderssen, E.L., Diep, D.B., Nes, I.F., Eijsink, V.G.H., Nissen-Meyer, J., 1998. Antagonistic activity of *Lactobacillus plantarum* C11: two new two-peptide bacteriocins, plantaricins EF and JK, and the induction factor plantaricin A. Appl. Environ. Microbiol. 64, 2269–2272. https://doi.org/10.1128/AEM.64.6.2269-2272.1998.

Arya, R., Kumari, S., Pandey, B., Mistry, H., Bihani, S.C., Das, A., Prashar, V., Gupta, G. D., Panicker, L., Kumar, M., 2021. Structural insights into SARS-CoV-2 proteins. J. Mol. Biol. 433, 166725. https://doi.org/10.1016/j.jmb.2020.11.024.

Balmeh, N., Mahmoudi, S., Fard, N.A., 2021. Manipulated bio antimicrobial peptides from probiotic bacteria as proposed drugs for COVID-19 disease. Inform. Med. Unlocked 23, 100515. https://doi.org/10.1016/j.imu.2021.100515.

Bansal, R., Mohagaonkar, S., Sen, A., Khanam, U., Rathi, B., 2021. In-silico study of peptide-protein interaction of antimicrobial peptides potentially targeting SARS and SARS-CoV-2 nucleocapsid protein. Silico Pharmacol 9, 46. https://doi.org/10.1007/s40203-021-00103-z.

Bhakat, S., Åberg, E., Söderhjelm, P., 2018. Prediction of binding poses to FXR using multi-targeted docking combined with molecular dynamics and enhanced sampling. J. Comput. Aided Mol. Des. 32, 59–73. https://doi.org/10.1007/s10822-017-0074-x.

Bhardwaj, V.K., Singh, R., Sharma, J., Rajendran, V., Purohit, R., Kumar, S., 2021. Identification of bioactive molecules from tea plant as SARS-CoV-2 main protease inhibitors. J. Biomol. Struct. Dyn. 39, 3449–3458. https://doi.org/10.1080/07391102.2020.1766572.

Biswas, S., Mahmud, S., Mita, M.A., Afrose, S., Hasan, MdR., Sultana, Shimu, Mst, S., Saleh, MdA., Mostafa-Hedeab, G., Alqarni, M., Obaidullah, A.J., Batiha, G.E.-S., 2022. Molecular docking and dynamics studies to explore effective inhibitory peptides against the spike receptor binding domain of SARS-CoV-2. Front. Mol. Biosci. 8, 791642. https://doi.org/10.3389/fmolb.2021.791642.

Blaszczyk, M., Ciemny, M.P., Kolinski, A., Kurcinski, M., Kmiecik, S., 2019. Protein–peptide docking using CABS-dock and contact information. Briefings Bioinf. 20, 2299–2305. https://doi.org/10.1093/bib/bby080.

Bruno, B.J., Miller, G.D., Lim, C.S., 2013. Basics and recent advances in peptide and protein drug delivery. Ther. Deliv. 4, 1443–1467. https://doi.org/10.4155/tde.13.104.

Chaalel, A., Riazi, A., Dubois-Dauphin, R., Thonart, P., 2015. Screening of plantaricin EF and JK in an Algerian Lactobacillus plantarum isolate. Asian Pacific Journal of Tropical Disease 5, 474–482. https://doi.org/10.1016/S2222-1808(15)60819-2.

Chen, Y., Liu, Q., Guo, D., 2020. Emerging coronaviruses: genome structure, replication, and pathogenesis. J. Med. Virol. 92, 418–423. https://doi.org/10.1002/jmv.25681.

Choi, H., Kang, H., Park, H., 2013. New solvation free energy function comprising intermolecular solvation and intramolecular self-solvation terms. J Cheminform 5, 8. https://doi.org/10.1186/1758-2946-5-8.

Chowdhury, N., Bagchi, A., 2022. Identification of the binding interactions of some novel antiviral compounds against Nsp1 protein from SARS-CoV-2 (COVID-19) through high throughput screening. J. Biomol. Struct. Dyn. 40, 6634–6641. https://doi.org/10.1080/07391102.2021.1887763.

Ciemny, M., Kurcinski, M., Kamel, K., Kolinski, A., Alam, N., Schueler-Furman, O., Kmiecik, S., 2018. Protein–peptide docking: opportunities and challenges. Drug Discov. Today 23, 1530–1537. https://doi.org/10.1016/j.drudis.2018.05.006.

Dassanayake, M.K., Khoo, T.-J., Chong, C.H., Di Martino, P., 2022. Molecular docking and in-silico analysis of natural biomolecules against dengue, ebola, zika, SARS-CoV-2 variants of concern and monkeypox virus. IJMS 23, 11131. https://doi.org/10.3390/ijms231911131.

De Lima Menezes, G., Da Silva, R.A., 2021. Identification of potential drugs against SARS-CoV-2 non-structural protein 1 (nsp1). J. Biomol. Struct. Dyn. 39, 5657–5667. https://doi.org/10.1080/07391102.2020.1792992.

Dey, D., Ema, T.I., Biswas, P., Aktar, S., Islam, S., Rinik, U.R., Firoz, M., Ahmed, S.Z., Azad, S.A., Rahman, A., Afrin, S., Mahedi, R.A., Badal, MdN.U., 2021. Antiviral effects of bacteriocin against animal-to-human transmittable mutated SARS-COV-2: a systematic review. Front. Agr. Sci. Eng. 8, 603. https://doi.org/10.15302/J-FASE-2021397.

Erol, I., Kotil, S.E., Fidan, O., Yetiman, A.E., Durdagi, S., Ortakci, F., 2023. In silico analysis of bacteriocins from lactic acid bacteria against SARS-CoV-2. Probiotics & Antimicro. Prot. 15, 17–29. https://doi.org/10.1007/s12602-021-09879-0.

Echegaray, N., Yilmaz, B., Sharma, H., Kumar, M., Pateiro, M., Ozogul, F., Lorenzo, J.M., 2023. A novel approach to Lactiplantibacillus plantarum: from probiotic properties to the omics insights. Microbiol. Res. 268, 127289. https://doi.org/10.1016/j.micres.2022.127289.

Ferreira De Freitas, R., Schapira, M., 2017. A systematic analysis of atomic protein–ligand interactions in the PDB. Med. Chem. Commun. 8, 1970–1981. https://doi.org/10.1039/C7MD00381A.

Genheden, S., Ryde, U., 2015. The MM/PBSA and MM/GBSA methods to estimate ligand-binding affinities. Expet Opin. Drug Discov. 10, 449–461. https://doi.org/10.1517/17460441.2015.1032936.

Gi Byun, W., Lee, M., Ko, M., Hyae Lee, J., Yi, S., Lee, J., Kim, S., Bum Park, S., 2024. Broad-Spectrum antiviral agents against SARS-CoV-2 variants inhibit the conserved viral protein nsp1–RNA interaction. Angew. Chem. Int. Ed. 63, e202405472. https://doi.org/10.1002/anie.202405472.

Güneş, Z.S., Çakır, B., Gülseren, İ., 2024. In silico prediction of preventive activities of bioactive hazelnut peptides against COVID -19 and Monkeypox 2022. Peptide Science 116, e24341. https://doi.org/10.1002/pep2.24341.

Gupta, S., Kapoor, P., Chaudhary, K., Gautam, A., Kumar, R., , Open Source Drug Discovery Consortium, Raghava, G.P.S., 2013. In silico approach for predicting toxicity of peptides and proteins. PLoS One 8, e73957. https://doi.org/10.1371/journal.pone.0073957.

Han, Y., Gao, Z., Chen, L., Kang, L., Huang, W., Jin, M., Wang, Q., Bae, Y.H., 2019. Multifunctional oral delivery systems for enhanced bioavailability of therapeutic peptides/proteins. Acta Pharm. Sin. B 9, 902–922. https://doi.org/10.1016/j.apsb.2019.01.004.

Jin, J., Wang, N., Wang, S., Alsaikhan, F., Ahmad, I., 2024. Targeting the main SARS-Cov-2 pathways with peptide inhibitors by molecular docking and molecular simulation approaches. J. Mol. Liq. 398, 124193. https://doi.org/10.1016/j.molliq.2024.124193.

Kamitani, W., Huang, C., Narayanan, K., Lokugamage, K.G., Makino, S., 2009. A two-pronged strategy to suppress host protein synthesis by SARS coronavirus Nsp1 protein. Nat. Struct. Mol. Biol. 16, 1134–1140. https://doi.org/10.1038/nsmb.1680.

Kc, S., 2024. Identification of potential SARS-CoV-2 Nsp1 inhibitors from Piper sarmentosum Roxb. using molecular docking. Trop. Biomed. 41, 166–175. https://doi.org/10.47665/tb.41.2.006.

Khramushin, A., Ben-Aharon, Z., Tsaban, T., Varga, J.K., Avraham, O., Schueler-Furman, O., 2022. Matching protein surface structural patches for high-resolution blind peptide docking. Proc. Natl. Acad. Sci. USA. 119, e2121153119. https://doi.org/10.1073/pnas.2121153119.

Kim, S.W., Kang, S.I., Shin, D.H., Oh, S.Y., Lee, C.W., Yang, Y., Son, Y.K., Yang, H.-S., Lee, B.-H., An, H.-J., Jeong, I.S., Bang, W.Y., 2020. Potential of cell-free supernatant from Lactobacillus plantarum NIBR97, including novel bacteriocins, as a natural alternative to chemical disinfectants. Pharmaceuticals 13, 266. https://doi.org/10.3390/ph13100266.

Kozakov, D., Hall, D.R., Xia, B., Porter, K.A., Padhorny, D., Yueh, C., Beglov, D., Vajda, S., 2017. The ClusPro web server for protein–protein docking. Nat. Protoc. 12, 255–278. https://doi.org/10.1038/nprot.2016.169.

Kurcinski, M., Jamroz, M., Blaszczyk, M., Kolinski, A., Kmiecik, S., 2015. CABS-dock web server for the flexible docking of peptides to proteins without prior knowledge of the binding site. Nucleic Acids Res. 43, W419–W424. https://doi.org/10.1093/nar/gkv456.

Laskowski, R.A., Jabłońska, J., Pravda, L., Vařeková, R.S., Thornton, J.M., 2018. PDBsum: structural summaries of PDB entries. Protein Sci. 27, 129–134. https://doi.org/10.1002/pro.3289.

Laskowski, R.A., Swindells, M.B., 2011. LigPlot+: multiple ligand–protein interaction diagrams for drug discovery. J. Chem. Inf. Model. 51, 2778–2786. https://doi.org/10.1021/ci200227u.

Lear, S., Cobb, S.L., 2016. Pep-Calc.com: a set of web utilities for the calculation of peptide and peptoid properties and automatic mass spectral peak assignment. J. Comput. Aided Mol. Des. 30, 271–277. https://doi.org/10.1007/s10822-016-9902-7.

Lee, D., Jung, H.G., Park, D., Bang, J., Cheong, D.Y., Jang, J.W., Kim, Y., Lee, S., Lee, S. W., Lee, G., Kim, Y.H., Hong, J.H., Hwang, K.S., Lee, J.H., Yoon, D.S., 2024. Bioengineered amyloid peptide for rapid screening of inhibitors against main protease of SARS-CoV-2. Nat. Commun. 15, 2108. https://doi.org/10.1038/s41467-024-46296-7.

Leffler, A.E., Kuryatov, A., Zebroski, H.A., Powell, S.R., Filipenko, P., Hussein, A.K., Gorson, J., Heizmann, A., Lyskov, S., Tsien, R.W., Poget, S.F., Nicke, A., Lindstrom, J., Rudy, B., Bonneau, R., Holford, M., 2017. Discovery of peptide ligands through docking and virtual screening at nicotinic acetylcholine receptor homology models. Proc. Natl. Acad. Sci. USA. 114. https://doi.org/10.1073/pnas.1703952114.

Ma, S., Damfo, S., Lou, J., Pinotsis, N., Bowler, M.W., Haider, S., Kozielski, F., 2022. Two ligand-binding sites on SARS-CoV-2 non-structural protein 1 revealed by fragment-based X-ray screening. IJMS 23, 12448. https://doi.org/10.3390/ijms232012448.

Mahmud, S., Biswas, S., Kumar Paul, G., Mita, M.A., Afrose, S., Robiul Hasan, Md, Sharmin Sultana Shimu, Mst, Uddin, M.A.R., Salah Uddin, Md, Zaman, S., Kaderi Kibria, K.M., Arif Khan, Md, Bin Emran, T., Abu Saleh, Md, 2021. Antiviral peptides against the main protease of SARS-CoV-2: a molecular docking and dynamics study. Arab. J. Chem. 14, 103315. https://doi.org/10.1016/j.arabjc.2021.103315.

Majumdar, G., Mandal, S., 2024. Evaluation of broad-spectrum antibacterial efficacy of quercetin by molecular docking, molecular dynamics simulation and in vitro studies. Chemical Physics Impact 8, 100501. https://doi.org/10.1016/j.chphi.2024.100501.

Mandal, M., Mandal, S., 2024a. MM-GBSA and QM/MM simulation-based in silico approaches for the inhibition of Acinetobacter baumannii class D OXA-24 β-lactamase using antimicrobial peptides melittin and RP-1. Chemical Physics Impact 8, 100401. https://doi.org/10.1016/j.chphi.2023.100401.

Mandal, M., Mandal, S., 2021. Molecular docking and dynamics simulation of L-hyoscyamine, eupatorium and alkaloid L27 as potential inhibitors against 3CLpro of SARS-CoV-2. Drug Discovery 15, 181–201. Available at: https://www.discoveryjournals.org/drugdiscovery/current_issue/2021/v15/n36/A6.htm. accessed 3.23.25.

Mandal, M., Mandal, S., 2024b. MM/GB(PB)SA integrated with molecular docking and ADMET approach to inhibit the fat-mass-and-obesity-associated protein using bioactive compounds derived from food plants used in traditional Chinese medicine. Pharmacological Research - Modern Chinese Medicine 11, 100435. https://doi.org/10.1016/j.prmcm.2024.100435.

Mandal, M., Mandal, S., 2024c. Metadynamics approach elucidating the free energy landscape and binding modes of vomicine with virulence factor towards anti-mpox drug discovery. Chem. Phys. Lett. 846, 141355. https://doi.org/10.1016/j.cplett.2024.141355.

Mercado-Camargo, J., Cervantes-Ceballos, L., Vivas-Reyes, R., Pedretti, A., Serrano-García, M.L., Gómez-Estrada, H., 2020. Homology modeling of leishmanolysin (gp63) from *Leishmania panamensis* and molecular docking of flavonoids. ACS Omega 5, 14741–14749. https://doi.org/10.1021/acsomega.0c01584.

Miller, B.R., McGee, T.D., Swails, J.M., Homeyer, N., Gohlke, H., Roitberg, A.E., 2012. *MMPBSA.py* : an efficient program for end-state free energy calculations. J. Chem. Theory Comput. 8, 3314–3321. https://doi.org/10.1021/ct300418h.

Min, Y.-Q., Mo, Q., Wang, J., Deng, F., Wang, H., Ning, Y.-J., 2020. SARS-CoV-2 nsp1: bioinformatics, potential structural and functional features, and implications for drug/vaccine designs. Front. Microbiol. 11, 587317. https://doi.org/10.3389/fmicb.2020.587317.

Moll, G.N., Van Den Akker, E., Hauge, H.H., Nissen-Meyer, J., Nes, I.F., Konings, W.N., Driessen, A.J.M., 1999. Complementary and overlapping selectivity of the two-peptide bacteriocins plantaricin EF and JK. J. Bacteriol. 181, 4848–4852. https://doi.org/10.1128/JB.181.16.4848-4852.1999.

Morozov, V., Rodrigues, C.H.M., Ascher, D.B., 2023. CSM-toxin: a web-server for predicting protein toxicity. Pharmaceutics 15, 431. https://doi.org/10.3390/pharmaceutics15020431.

Morris, A.L., MacArthur, M.W., Hutchinson, E.G., Thornton, J.M., 1992. Stereochemical quality of protein structure coordinates. Proteins 12, 345–364. https://doi.org/10.1002/prot.340120407.

Omer, A.A.M., Hinkula, J., Tran, P.-T.-H., Melik, W., Zattarin, E., Aili, D., Selegård, R., Bengtsson, T., Khalaf, H., 2022. Plantaricin NC8 αβ rapidly and efficiently inhibits flaviviruses and SARS-CoV-2 by disrupting their envelopes. PLoS One 17, e0278419. https://doi.org/10.1371/journal.pone.0278419.

Omer, A.A.M., Kumar, S., Selegård, R., Bengtsson, T., Khalaf, H., 2025. Characterization of novel plantaricin-derived antiviral peptides against flaviviruses. IJMS 26, 1038. https://doi.org/10.3390/ijms26031038.

Panigrahi, S.K., Desiraju, G.R., 2007. Strong and weak hydrogen bonds in the protein–ligand interface. Proteins 67, 128–141. https://doi.org/10.1002/prot.21253.

Piotto, S.P., Sessa, L., Concilio, S., Iannelli, P., 2012. YADAMP: yet another database of antimicrobial peptides. Int. J. Antimicrob. Agents 39, 346–351. https://doi.org/10.1016/j.ijantimicag.2011.12.003.

Pourmand, S., Zareei, S., Shahlaei, M., Moradi, S., 2022. Inhibition of SARS-CoV-2 pathogenesis by potent peptides designed by the mutation of ACE2 binding region. Comput. Biol. Med. 146, 105625. https://doi.org/10.1016/j.compbiomed.2022.105625.

Protić, S., Kaličanin, N., Sencanski, M., Prodanović, O., Milicevic, J., Perovic, V., Paessler, S., Prodanović, R., Glisic, S., 2023. In silico and in vitro inhibition of SARS-CoV-2 PLpro with gramicidin D. IJMS 24, 1955. https://doi.org/10.3390/ijms24031955.

Rajpoot, S., Solanki, K., Kumar, A., Zhang, K.Y.J., Pullamsetti, S.S., Savai, R., Faisal, S.M., Pan, Q., Baig, M.S., 2022. In-silico design of a novel tridecapeptide targeting spike protein of SARS-CoV-2 variants of concern. Int J Pept Res Ther 28, 28. https://doi.org/10.1007/s10989-021-10339-0.

Ramirez-Acosta, K., Rosales-Fuerte, I.A., Perez-Sanchez, J.E., Nuñez-Rivera, A., Juarez, J., Cadena-Nava, R.D., 2022. Design and selection of peptides to block the SARS-CoV-2 receptor binding domain by molecular docking. Beilstein J. Nanotechnol. 13, 699–711. https://doi.org/10.3762/bjnano.13.62.

Razali, R., Asis, H., Budiman, C., 2021. Structure-function characteristics of SARS-CoV-2 proteases and their potential inhibitors from microbial sources. Microorganisms 9, 2481. https://doi.org/10.3390/microorganisms9122481.

Rogne, P., Haugen, C., Fimland, G., Nissen-Meyer, J., Kristiansen, P.E., 2009. Three-dimensional structure of the two-peptide bacteriocin plantaricin JK. Peptides 30, 1613–1621. https://doi.org/10.1016/j.peptides.2009.06.010.

Sadremomtaz, A., Al-Dahmani, Z.M., Ruiz-Moreno, A.J., Monti, A., Wang, C., Azad, T., Bell, J.C., Doti, N., Velasco-Velázquez, M.A., De Jong, D., De Jonge, J., Smit, J., Dömling, A., Van Goor, H., Groves, M.R., 2022. Synthetic peptides that antagonize the angiotensin-converting enzyme-2 (ACE-2) interaction with SARS-CoV-2 receptor binding spike protein. J. Med. Chem. 65, 2836–2847. https://doi.org/10.1021/acs.jmedchem.1c00477.

Selvaraju, G., Leow, T.C., Salleh, A.B., Normi, Y.M., 2020. Design and characterisation of inhibitory peptides against Bleg1_2478, an evolutionary divergent B3 metallo-β-lactamase. Molecules 25, 5797. https://doi.org/10.3390/molecules25245797.

Sharma, N., Patiyal, S., Dhall, A., Pande, A., Arora, C., Raghava, G.P.S., 2021a. AlgPred 2.0: an improved method for predicting allergenic proteins and mapping of IgE epitopes. Briefings Bioinf. 22, bbaa294. https://doi.org/10.1093/bib/bbaa294.

Sharma, J., Kumar Bhardwaj, V., Singh, R., Rajendran, V., Purohit, R., Kumar, S., 2021b. An in-silico evaluation of different bioactive molecules of tea for their inhibition potency against non structural protein-15 of SARS-CoV-2. Food Chem. 346, 128933. https://doi.org/10.1016/j.foodchem.2020.128933.

Singh, R., Bhardwaj, V.K., Purohit, R., 2022. Inhibition of nonstructural protein 15 of SARS-CoV-2 by golden spice: a computational insight. Cell Biochem. Funct. 40, 926–934. https://doi.org/10.1002/cbf.3753.

Singh, R., Bhardwaj, V.K., Purohit, R., 2021a. Potential of turmeric-derived compounds against RNA-dependent RNA polymerase of SARS-CoV-2: an in-silico approach. Comput. Biol. Med. 139, 104965. https://doi.org/10.1016/j.compbiomed.2021.104965.

Singh, R., Bhardwaj, V.K., Sharma, J., Kumar, D., Purohit, R., 2021b. Identification of potential plant bioactive as SARS-CoV-2 Spike protein and human ACE2 fusion inhibitors. Comput. Biol. Med. 136, 104631. https://doi.org/10.1016/j.compbiomed.2021.104631.

Singh, R., Purohit, R., 2024. Multi-target approach against SARS-CoV -2 by stone apple molecules: a master key to drug design. Phytother Res. 38, 7–10. https://doi.org/10.1002/ptr.7772.

Sobolev, O.V., Afonine, P.V., Moriarty, N.W., Hekkelman, M.L., Joosten, R.P., Perrakis, A., Adams, P.D., 2020. A global ramachandran score identifies protein structures with unlikely stereochemistry. Structure 28, 1249–1258.e2. https://doi.org/10.1016/j.str.2020.08.005.

Souza, P.F.N., Lopes, F.E.S., Amaral, J.L., Freitas, C.D.T., Oliveira, J.T.A., 2020. A molecular docking study revealed that synthetic peptides induced conformational changes in the structure of SARS-CoV-2 spike glycoprotein, disrupting the interaction with human ACE2 receptor. Int. J. Biol. Macromol. 164, 66–76. https://doi.org/10.1016/j.ijbiomac.2020.07.174.

Sundar, S., Thangamani, L., Piramanayagam, S., Rahul, C.N., Aiswarya, N., Sekar, K., Natarajan, J., 2021. Screening of FDA-approved compound library identifies potential small-molecule inhibitors of SARS-CoV-2 non-structural proteins NSP1, NSP4, NSP6 and NSP13: molecular modeling and molecular dynamics studies. J Proteins Proteom 12, 161–175. https://doi.org/10.1007/s42485-021-00067-w.

Tallei, T.E., Fatimawali, Yelnetty, A., Idroes, R., Kusumawaty, D., Emran, T.B., Yesiloglu, T.Z., Sippl, W., Mahmud, S., Alqahtani, T., Alqahtani, A.M., Asiri, S., Rahmatullah, M., Jahan, R., Khan, MdA., Celik, I., 2021. An analysis based on molecular docking and molecular dynamics simulation study of bromelain as anti-SARS-CoV-2 variants. Front. Pharmacol. 12, 717757. https://doi.org/10.3389/fphar.2021.717757.

Teiar, R., Sane, F., Erol, I., Nekoua, M.P., Lecouturier, D., Boukherroub, R., Durdağı, S., Hober, D., Drider, D., 2024. Enterocin DD14 can inhibit the infection of eukaryotic cells with enveloped viruses. Arch. Microbiol. 206, 269. https://doi.org/10.1007/s00203-024-04002-7.

Thoms, M., Buschauer, R., Ameismeier, M., Koepke, L., Denk, T., Hirschenberger, M., Kratzat, H., Hayn, M., Mackens-Kiani, T., Cheng, J., Straub, J.H., Stürzel, C.M., Fröhlich, T., Berninghausen, O., Becker, T., Kirchhoff, F., Sparrer, K.M.J., Beckmann, R., 2020. Structural basis for translational shutdown and immune evasion by the Nsp1 protein of SARS-CoV-2. Science 369, 1249–1255. https://doi.org/10.1126/science.abc8665.

Udenigwe, C.C., Fogliano, V., 2017. Food matrix interaction and bioavailability of bioactive peptides: two faces of the same coin? J. Funct.Foods 35, 9–12. https://doi.org/10.1016/j.jff.2017.05.029.

Valdés-Tresanco, M.S., Valdés-Tresanco, M.E., Valiente, P.A., Moreno, E., 2021. gmx_MMPBSA: a new tool to perform end-state free energy calculations with GROMACS. J. Chem. Theory Comput. 17, 6281–6291. https://doi.org/10.1021/acs.jctc.1c00645.

Vittorio, S., Lunghini, F., Morerio, P., Gadioli, D., Orlandini, S., Silva, P., Jan, Martinovic, Pedretti, A., Bonanni, D., Del Bue, A., Palermo, G., Vistoli, G., Beccari, A.R., 2024. Addressing docking pose selection with structure-based deep learning: recent advances, challenges and opportunities. Comput. Struct. Biotechnol. J. 23, 2141–2151. https://doi.org/10.1016/j.csbj.2024.05.024.

Wang, L., Wang, N., Zhang, W., Cheng, X., Yan, Z., Shao, G., Wang, X., Wang, R., Fu, C., 2022. Therapeutic peptides: current applications and future directions. Sig Transduct Target Ther 7, 48. https://doi.org/10.1038/s41392-022-00904-4.

Xu, Y., Yang, L., Li, P., Gu, Q., 2019. Heterologous expression of class IIb bacteriocin plantaricin JK in Lactococcus lactis. Protein Expr. Purif. 159, 10–16. https://doi.org/10.1016/j.pep.2019.02.013.

Xue, L.C., Rodrigues, J.P., Kastritis, P.L., Bonvin, A.M., Vangone, A., 2016. PRODIGY: a web server for predicting the binding affinity of protein–protein complexes. Bioinformatics 32, 3676–3678. https://doi.org/10.1093/bioinformatics/btw514.

Yan, W., Zheng, Y., Zeng, X., He, B., Cheng, W., 2022. Structural biology of SARS-CoV-2: open the door for novel therapies. Sig Transduct Target Ther 7, 26. https://doi.org/10.1038/s41392-022-00884-5.